JOURNAL OF GEOPHYSICAL RESEARCH, VOL. 93, NO. A10, PAGES 11,405–11,428, OCTOBER 1, 1988

Transverse Ion Energization and Low-Frequency Plasma Waves in the Mid-Altitude Auroral Zone: A Case Study

W. K. PETERSON,[1] E. G. SHELLEY,[1] S. A. BOARDSEN,[2] D. A. GURNETT,[2] B. G. LEDLEY,[3] M. SUGIURA,[4] T. E. MOORE,[5] AND J. H. WAITE [5,6]

The transport of ions from the ionosphere to the magnetosphere requires that ions acquire significant energy in directions both transverse and parallel to the magnetic field. There is a considerable body of experimental evidence that shows that transverse energization occurs over a wide range of altitudes on auroral field lines. Many recent analytical and simulation studies have addressed the microphysics involved in transverse ion energization. There are, however, remarkably few published high-resolution plasma and plasma wave observations obtained in the mid-altitude auroral region available to compare with the analytical and simulation studies. Several hundred hours of high-resolution plasma data obtained from the Dynamics Explorer 1 satellite have been surveyed. A wide variety of plasma environments that are difficult to simply characterize were found. We present here a comprehensive set of high-sensitivity, high-resolution plasma wave, ion, and magnetometer data obtained from an evening auroral zone crossing at $r/R_E \sim 3$. The total density, thermal structure, and composition of the plasma in this representative interval varied rapidly, as did the character (mode) of low-frequency plasma waves observed. We did not find an unambiguous particle and wave signature of local transverse ion energization, but we did frequently find intervals where local transverse ion heating was consistent with the observations. We also found a downward flowing ion distribution that occurred simultaneously with a region of intense plasma wave emissions primarily below the lower hybrid resonance frequency.

INTRODUCTION

It is now well established that ions of ionospheric origin contribute significantly to magnetospheric plasmas. The available evidence from over a decade of ion mass spectrometer measurements in all regions of the magnetosphere indicates that the transfer of the majority of energetic ions (i.e., ions with energies greater than $\sim$ 10 eV) from the ionosphere to the magnetosphere occurs on auroral field lines (see, for example, *Shelley* [1986] and *Yau et al.* [1984, 1985*a*,*b*]). One of the current themes in space plasma physics research is the attempt to understand the physical processes responsible for energization of very low energy ionospheric ions to energies of kilovolts in the auroral zone. These processes determine to a large extent the nature and strength of the coupling of the Earth's ionospheric and magnetospheric plasmas. To date, two broad classes of ion acceleration mechanisms have been identified. These mechanisms differ in that one class imparts energy to ions in a direction parallel to the Earth's magnetic field and the other imparts energy to ions transverse to the magnetic field. In this report we consider transverse ion energization and associated low-frequency plasma waves.

Transverse ion energization or acceleration has been observed in almost all regions of the magnetosphere from altitudes of several hundred kilometers in the auroral ionosphere (see, for example, *Yau et al.* [1983]), in the mid-altitude auroral zone [*Sharp et al.*, 1977], and in the Earth's magnetotail [*Sharp et al.*, 1981]. It is generally assumed that low-frequency (i.e., below a few thousand hertz) plasma waves are associated with transverse energization of ions (see, for example, *Ungstrup et al.*, [1979] *Chang* and *Coppi* [1981] and *Lysak* [1986]). The interactions between ions and low-frequency plasma waves are varied and complex, especially in the tenuous plasmas in the diverging magnetic field found at mid-altitudes in the auroral zone. In spite of many years of research, our understanding of the physical processes involved in the interchange of energy between plasma waves and ions on auroral field lines is incomplete. *Kintner* [1986] in a recent review has emphasized the difficulties involved in interpreting low-frequency plasma wave data obtained in the auroral zone. *Kintner and Gorney* [1984] have pointed out that suitable events for detailed analysis of transverse ion energization are found only rarely in existing satellite data sets. A digest and comprehensive bibliography on the subject was recently compiled by *Klumpar* [1986].

The unambiguous signature of localized transverse ion energization is an ion angular distribution that peaks in a direction perpendicular to the local magnetic field—the so-called 90° conic distribution. Kintner and Gorney found only one such event in the S3-3 data set where broadband plasma wave measurements were obtained simultaneously with particle data. In the data surveyed for this report, no 90° ion conic distributions were found. The ninety degree ion conic is not a unique signature of local transverse ion acceleration or energization, however. *Lysak et al.* [1980], *Chang et al.* [1986], *Temerin* [1986] and others have considered ion heating over extended altitude regions by various mechanisms and commented on how assumptions on the heating mechanisms, heating rates, and altitude distribution of heating modify expected ion distributions. Recent observations have confirmed the nonuniqueness of the 90° ion conic distribution as a local signature of transverse ion heating or acceleration. *Klumpar et al.* [1984] interpreted observations of ion distributions obtained with the ion mass spectrometer on DE 1 in terms of a bimodal acceleration, i.e., both transverse and parallel acceleration occurring on the same field line and near the same altitude. Observations of *Chang et al.* [1986] also from Dynamics Explorer have been interpreted in terms of an energization mechanism that operates over an extended altitude region.

[1]Lockheed Palo Alto Research Laboratory, Palo Alto, California.
[2]University of Iowa, Iowa City.
[3]NASA Goddard Space Flight Center, Greenbelt, Maryland.
[4]Geophysical Institute, Kyoto University, Kyoto, Japan.
[5]NASA Marshall Space Flight Center, Huntsville, Alabama.
[6]Now at Department of Space Sciences, Southwest Research Institute, San Antonio, Texas.

Paper number 8A9501.
0148-0227/88/008A-9501$05.00

TABLE 1. Dynamics Explorer 1 Instruments Used to Obtain the Plasma Parameters Reported Here

Instrument package	Acronym	Plasma Parameters
Plasma wave instrument *Shawhan et al.* [1981]	PWI	Low-resolution plasma wave emissions from a swept frequency analyzer (1 Hz to 500 kHz), once per 32 s from electric and magnetic antennas. Correlation of in-phase and quadrature-phase signals from electric and magnetic antennas. Plasma densities deduced from the SFR data. 0- to 10-kHz wideband plasma wave data.
Energetic ion mass spectrometer *Shelley et al.* [1981]	EICS	Ion energy-angle spectra over the range 10 eV to 17 keV for hydrogen and oxygen every 24 s for all pitch angles. Partial densities, and perpendicular plasma pressures deduced from energy-angle spectra. 6-s resolution energy-angle samples of single mass species over a restricted energy range.
Retarding ion mass spectrometer *Chappell et al.* [1981]	RIMS	Ion energy spectra from spacecraft potential to 50 eV from a wide field of view transverse to the local magnetic field with 1-min time resolution for hydrogen, oxygen, and singly charged helium. Relative composition deduced from these spectra. Ion angle spectra for all energies from spacecraft potential to 50 eV for all pitch angles.
Magnetometer *Farthing et al.* [1981]	MAG	Three-dimensional magnetometer measurements with 6-s resolution. Field aligned currents deduced from these measurements.

There are now a number of plasma simulations of transverse heating of auroral ions in various regions of the aurora that take into account the variability of the plasma environment on auroral field lines (see, for example, *Ashour-Abdalla et al.* [1988]). These simulations have been primarily motivated by observations reported from the S3-3 satellite. Given our evolving understanding of transverse ion acceleration process and the high-resolution plasma instrumentation on the Dynamics Explorer (DE) 1 satellite, it is appropriate to reexamine the experimental observations of transverse ion energization at altitudes of several Earth radii in the auroral zone.

This report is organized as follows. We first briefly discuss the plasma instrumentation used. We then show how the complexity and volume of data lead us to present very high resolution data from only one auroral zone crossing. The data from the selected interval are presented, and two independent criteria are used to select possible localized regions where energetic ions are transversely heated. We then discuss the plasma environment in three selected intervals. We demonstrate that the data are consistent with the local transfer of energy to the ions in two of these intervals. However, we were not able to unambiguously show that any of these intervals were the site of a significantly enhanced transfer of energy from plasma waves to ions. The discussion section further illustrates the difficulties encountered in our attempts to determine the precise nature of space plasma processes using current instrumentation.

PLASMA INSTRUMENTATION

The Dynamics Explorer 1 satellite was launched on August 3, 1981, into an elliptic polar orbit with an apogee of $r/R_E \sim 4.6$ [*Hoffman et al.*, [1981]. The instruments on the DE 1 satellite provide high-resolution plasma wave and ion mass spectrometer measurements over extended frequency and energy ranges. Data from four of the six instrument packages on DE 1 are presented here. The energetic ion composition spectrometer (EICS) was operated in a mode that returned a 24-point angular distribution for 15 selected energy bands covering the range from 10 eV to 17 keV for hydrogen and oxygen every 24 s or four satellite spin periods. Higher time resolution, at the expense of mass coverage and energy resolution, was available. During each satellite spin period (6 s), data were obtained from one mass (hydrogen or oxygen), 24 pitch angles, and half of the complete set of energy bands. The retarding ion mass spectrometer (RIMS) instrument extended ion mass spectrometer coverage below 10 eV. The plasma wave instrument (PWI) wideband receiver was operated in a mode that provided coverage from near dc to 10 kHz. Because of operational considerations, PWI wideband data in the 0.01- to 10-kHz mode were not obtained systematically before January 1984 and for only a small subset of the data acquisition intervals after then. During the time period of the study reported here the PWI swept frequency analyzer and magnetometer were operated in standard modes. Electron measurements are not available for any of the intervals surveyed in the preparation of this report. However, field-aligned current measurements inferred from magnetometer measurements provide some insight into the ambient electron plasma.

A listing of the instruments used and the plasma parameters measured are shown in Table 1. Note that each of the instrument packages on DE 1 has many operational modes; the entries in Table 1 refer only to the instrumental modes used in the data intervals discussed here. Complete descriptions of the instruments as well as the Dynamics Explorer program are found in papers listed in Table 1.

DATA SELECTION AND PRESENTATION

Starting in early 1984, a coordinated set of high time resolution plasma and plasma wave observations from the Earth's polar regions including the auroral zone and cusp were systematically acquired by instruments on the Dynamics Explorer 1 satellite. A few intervals were identified in a preliminary scan of this data set which were characterized by intense, extended regions of plasma wave emissions spaced at the local hydrogen gyrofrequency and for which high time resolution energetic ion composition spectrometer (EICS) data were available. *Peterson et al.* [1986] presented a comparison of the wideband plasma wave and energetic ion composition data for several of these events and showed that it was not uncommon for both H^+ and O^+ ions to have extra transverse energy where only hydrogen ion cyclotron emissions were detectable. Data from the full complement of plasma instruments operating on the Dynamics Explorer 1 satellite were assembled for several of the data intervals used in the *Peterson et al.* [1986] study and are the basis of this report.

Unambiguous identification of regions where transverse ion heating and/or acceleration is occurring at the mid-auroral altitudes sampled by Dynamics Explorer 1 has proven to be difficult. Energetic ion distributions peaked perpendicular to the local magnetic field, the so-called 90° ion conic distributions, unambiguously identify regions of local transverse ion energization (see, for

example, *Kintner and Gorney* [1984]). To date, only one such 90° ion conic distribution has been found in the Dynamics Explorer data but not at a time during which low-frequency, high-resolution plasma wave data were acquired. As noted in the introduction, 90° ion conic distributions are sufficient but not necessary signatures of transverse ion energization. If there is an intense background of quasi-isotropic hot ions, if the intensity of the transversely energized ions is below an instrumental threshold, or if transverse energization occurs over an extended altitude region, 90° ion conics will either not be produced or not be detected.

To identify regions of possible transverse ion energization we have used two independent criteria: (1) intense low-frequency plasma wave emissions and (2) local maxima in the energetic ion plasma pressure. (The reason for using plasma pressure rather than plasma temperature is discussed below.) Several hundred hours of wideband data from the plasma wave instrument (PWI) were examined at highest time resolution for regions of intense low-frequency plasma wave activity. A few hours ($\sim$ 10) of energetic ion data were processed, and moments of the ion distributions were searched for regions of local maxima in the plasma pressure transverse to the magnetic field. As in previous studies of transverse ion energization in space plasmas, the assembled data were diverse and difficult to characterize. The same set of "events" were not selected by both criteria. Some regions of intense plasma wave emission were found associated with sharp gradients in ion density and temperature where it was not possible to characterize the ion plasma because of the relatively long instrumental cycle times. A third possible indicator of transverse ion energization, field-aligned currents, was generally not correlated with either intense low-frequency plasma wave emissions or local maxima in the transverse plasma pressure.

The energetic ion and plasma wave data observed during the periods selected for this study were typical of those found in the mid-altitude auroral zone. That is, the geomagnetic conditions were not extremely quiet or disturbed, and the relatively low resolution summary spectrograms did not show unusual features. Intervals with near-simultaneous local maxima in both low-frequency plasma wave emissions and partial perpendicular ion pressure were identified in a number of mid-altitude auroral zone crossings. We frequently found the data in these selected intervals were consistent with the occurrence of local transfer of transverse energy to ions. However, our analysis of the plasma parameters in these intervals did not reveal a single event where we were able to unambiguously identify the local transfer of energy from plasma waves to ions.

It is difficult to simply summarize the high-resolution data surveyed. First, a very large volume of high-resolution data are needed to characterize time intervals of interest because we do not yet know how to simply and compactly present the data necessary to determine the plasma wave emission mode or shape of the ion velocity space distribution with the required temporal resolution. Second, the observed plasma environment in the mid-altitude auroral zone is extremely variable. We determined that the most efficient way to present the results of our study was to present the high-resolution plasma measurements for one crossing of the mid-altitude auroral zone. It is true that no one auroral zone crossing interval can show the full variety and complexity of the data; however, we feel that it is more illuminating to show in detail the variability of data acquired during a single mid-altitude auroral zone crossing than to present a summary of the variability of data acquired over several months.

The interval selected for detailed presentation occurred between 1430 and 1500 UT on January 4, 1984, and was characterized by moderate magnetic activity. The 3-hour magnetic activity index, *Kp*, for the 1200 to 1500 UT interval was 3; the hourly average auroral electrojet (*AE*) index was 287 between 1400 and 1500 UT. Earlier in the day, near 0700 UT, there was considerable magnetic activity; *Kp* was 6 and the hourly *AE* index 892. Plate 1 is a color spectrogram displaying 2 hours of the plasma wave instrument (PWI) swept frequency receiver (SFR) response from the electric (top) and magnetic loop (bottom) antennas obtained on January 4, 1984. The intensities of plasma emissions detected have been encoded using the color scales indicated on the right and displayed as a function of frequency (1 Hz to 400 kHz) and time. An extensive discussion on the plasma waves normally encountered at this altitude in the evening auroral zone and a more complete discussion of the format of Plate 1 have been given by *Gurnett et al.*, [1983]. Note in particular the two auroral zone crossings centered on 1410 and 1440 and the very weak signal in the magnetic antenna after $\sim$ 1420 UT. The data displayed in Plate 1 are typical of those found in this local time and altitude region. Very high spectral resolution plasma wave data over the range from a few hertz to 10 kHz (the so called wideband data) from the PWI instrument are available only for the interval 1427 to 1502 UT. We have therefore selected the second crossing of the auroral zone on this pass for detailed examination.

Figure 1 is an energy-time spectrogram showing the energetic ion plasma detected by the energetic ion mass spectrometer (EICS) for part of the period shown in Plate 1. The spin-averaged number flux in units of $(cm^2\ s\ sr\ keV)^{-1}$ for H^+ and O^+ (M/Q = 1 and 16 respectively) has been encoded using the gray bar shown on the right. The ordinate of each panel covers the energy range sampled (10 eV to 17 keV). Gray scale coded energy spectra are presented for both species sampled for each EICS instrument cycle (24 s) from $\sim$ 1415 UT when DE 1 was in the polar cap to $\sim$ 1540 UT when DE 1 was equatorward of the main region of auroral activity. Note that H^+ ions of $\sim$ 1 keV energy were above the EICS sensitivity threshold after $\sim$ 1440 UT, and detectable O^+ ions of the same energy were not encountered until $\sim$ 1450 UT. We will show below that the interval before $\sim$ 1442 UT is dominated by cool plasma, i.e., the most intense fluxes of ions are at energies below $\sim$ 10 eV. The energetic ions encountered on this auroral zone crossings have energy and angular distributions similar to those seen on many other auroral zone crossing in this local time sector. We note here that energies of the upflowing ions seen on this auroral crossing are low and would not have been detected by the ion mass spectrometer on the S3-3 satellite [*Ghielmetti et al.*, 1978; *Collin and Johnson*, 1985], but would have been seen by the non-mass-discriminating electrostatic ion analyzer on the same satellite [*Gorney et al.*, 1981].

Some of the data used to identify regions of possible transverse ion energization are presented in Figure 2 as a function of time. The satellite location (magnetic local time, invariant latitude, and geocentric distance) are also indicated. The top panel presents the root-mean-square (Rms) voltage detected on the long-wire electric antenna in the frequency range 0.01 to 1 kHz. Intense regions of low-frequency plasma wave emissions are seen at 1439, 1441:30, 1442:30, 1445 and 1451:30 UT. The second and third panels in Figure 2 display partial ion temperatures (in units of keV) perpendicular to the magnetic field calculated from moments of the measured energetic hydrogen and oxygen ion velocity space distributions. The three-dimensional moment integrals are approximated by sums of the EICS measurements made in the two- dimensional spin plane. Extrapolation to the third dimension is done by assuming gyrotropy, i.e., that the plasma is organized by the magnetic field and plasma drift across magnetic field lines is not a dominant

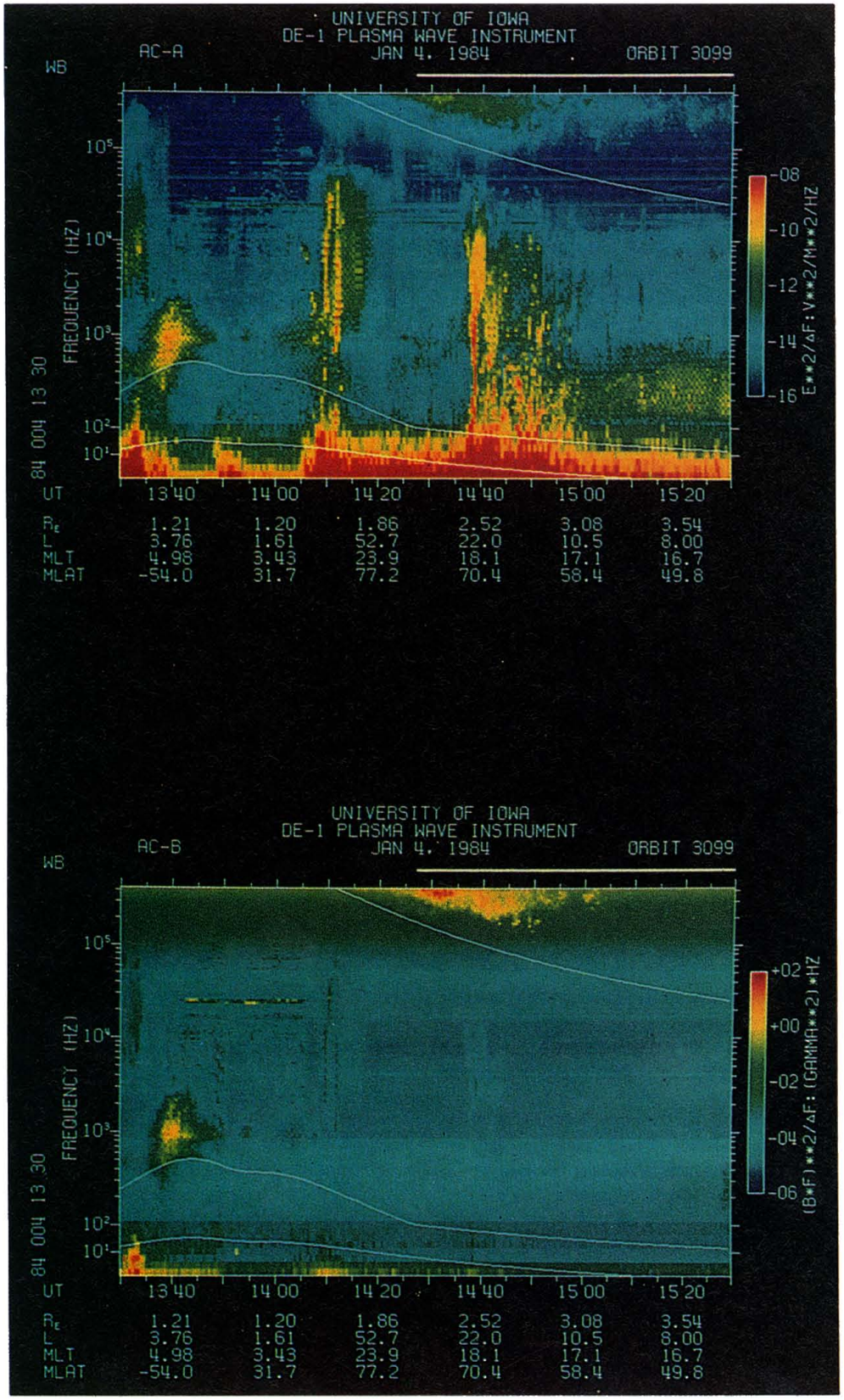

Plate 1. Plasma wave emissions observed for 2 hours on January 4, 1984, from the plasma wave instrument (PWI) swept frequency receiver (SFR). Response from the electric (top) and magnetic loop (bottom) antennas has been encoded using the intensity scales on the right and displayed as a function of frequency (1 Hz to 400 kHz) and time. An extensive discussion on the plasma waves normally encountered at this altitude in the evening auroral zone and a more complete discussion of the format of Plate 1 have been given by *Gurnett et al.* [1983]. The satellite position as a function universal time (UT) is given at the bottom in geocentric distance (R_E), McIlwain "L" parameter, magnetic local time (MLT), and geomagnetic latitude (MLAT).

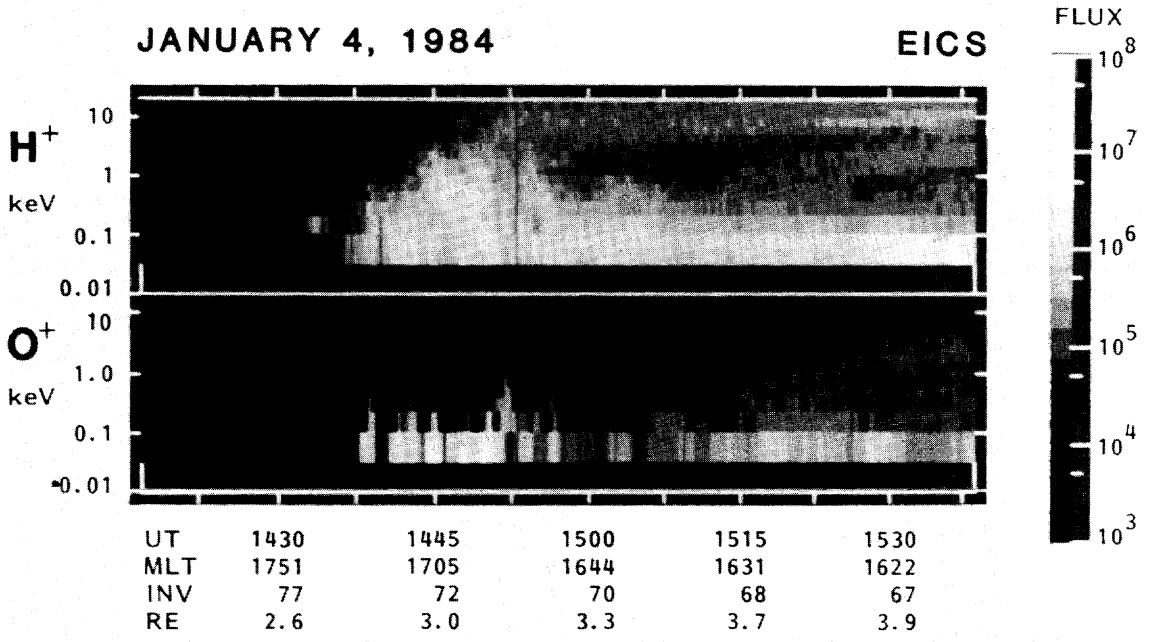

Fig. 1. Energetic ions observed for part of the interval displayed in Plate 1 in energy-time spectrogram format. The spin averaged number flux in units of $(cm^2\ s\ sr\ keV)^{-1}$ for H^+ and O^+ (M/Q = 1 and 16 respectively) has been encoded using the gray bar shown on the right. The ordinate of each panel covers the energy range sampled (10 eV to 17 keV). The satellite position is indicated at the bottom in magnetic local time (MLT), invariant latitude (INV), and geocentric distance (R_E).

effect. We have restricted the energy range used to calculate the ion moments to the range 150 eV/e < E/q < 17 keV/e to avoid having to make assumptions about the energy dependence of the measured distribution function within the very broad lowest- energy channel of the EICS instrument (10 eV to ~ 125 eV for the data presented here). The fourth and fifth panels present the partial ion pressure (perpendicular temperature times partial ion density) for hydrogen and oxygen in units of keV/cm^3. Features in the transverse ion temperature plots do not correspond to regions of intense low-frequency plasma wave activity indicated in the first panel, but there is a correlation between regions of low-frequency plasma wave emissions (top panel) and some features in the partial perpendicular hydrogen pressure. Ion temperatures determined from ion measurements at energies above 150 eV are not a good indicator of localized regions of transverse ion energization because ion plasma encountered on auroral field lines is a variable mixture of cool (i.e., less than 100 eV) ambient and upflowing ionospheric plasma and downflowing, precipitating, and mirroring plasma sheet plasmas. The observed systematic variations of the thermal structure of the ion plasma is discussed more fully below. Here we note that local maxima in the partial perpendicular hydrogen pressure are seen near 1439, 1440:30, 1442:30, 1444, 1445:30, 1447:30 and 1449 UT. Several small features are also seen after 1449 UT. Some, but not all, local maxima in hydrogen partial perpendicular pressure correspond to simultaneous local maxima in the partial perpendicular oxygen pressure.

Intense large-scale field-aligned currents can lead to plasma instabilities that in turn will transversely heat a local ion population (see, for example *Kindel and Kennel*, [1971]; and *Cattell*, [1981]). Both large-scale and small-scale field-aligned current sheets are encountered during the period of interest. The bottom two panels in Figure 2 present 6 s averages of data obtained from the high-resolution magnetometer. Large-scale field-aligned currents can be identified in the bottom panel which displays the difference between a model and the measured phi component of the magnetic field. The phi component is oriented in the east-west geomagnetic direction and is sensitive to large-scale field-aligned currents. A positive slope in the difference of the measured and modeled phi components of the magnetic field with decreasing invariant latitude implies a current out of the ionosphere, and a negative slope implies a current into the ionosphere. The general increase in the delta phi component seen in this interval is believed to be associated with (1) uncertainties in the knowledge of the magnetometer sensor's attitude and (2) limitations inherent in the use of magnetic field models. It is clear, however, that times near ~ 1439, and ~ 1443 UT are at boundaries of large-scale field-aligned current sheets. The poleward current sheet observed from ~ 1439 to ~ 1443 UT has the polarity of a current into the ionosphere. Such currents are generally believed to be carried by thermal electrons flowing up magnetic field lines from the ionosphere. Statistical studies of large-scale field- aligned currents at ionospheric altitudes [*Iijima and Potemra*, 1978] show that poleward current sheets of this polarity are commonly observed at later magnetic local times (i.e., after 2100 UT). The region 1 upward field-aligned current sheet starts at ~ 1443 UT, but its equatorward boundary and the start of the region 2 downward field-aligned current sheet are either after 1453 UT (i.e., below 70° invariant latitude) or masked by the general increase with decreasing latitude in the delta phi component shown in Figure 2. The expected location of the boundary between region 1 and 2 current sheets at 1800 hours magnetic local time is ~ 68° invariant latitude [*Iijima and Potemra*, 1978]. The interval from ~ 1446 to ~ 1449 UT, which is discussed at length below, is clearly in a region of upward field-aligned currents. Ignoring the small-scale variations in the magnetic field phi component, we can estimate the average magnitude of the downward field-aligned currents at ~ 4×10^{-8} A/m^2 over the interval 1439 to 1444 UT and ~ 6×10^{-8} A/m^2 for the upward, region 1 currents if they extend from 1444 to 1454 UT. In the absence of parallel electric fields below the satellite, the field-aligned current density at the

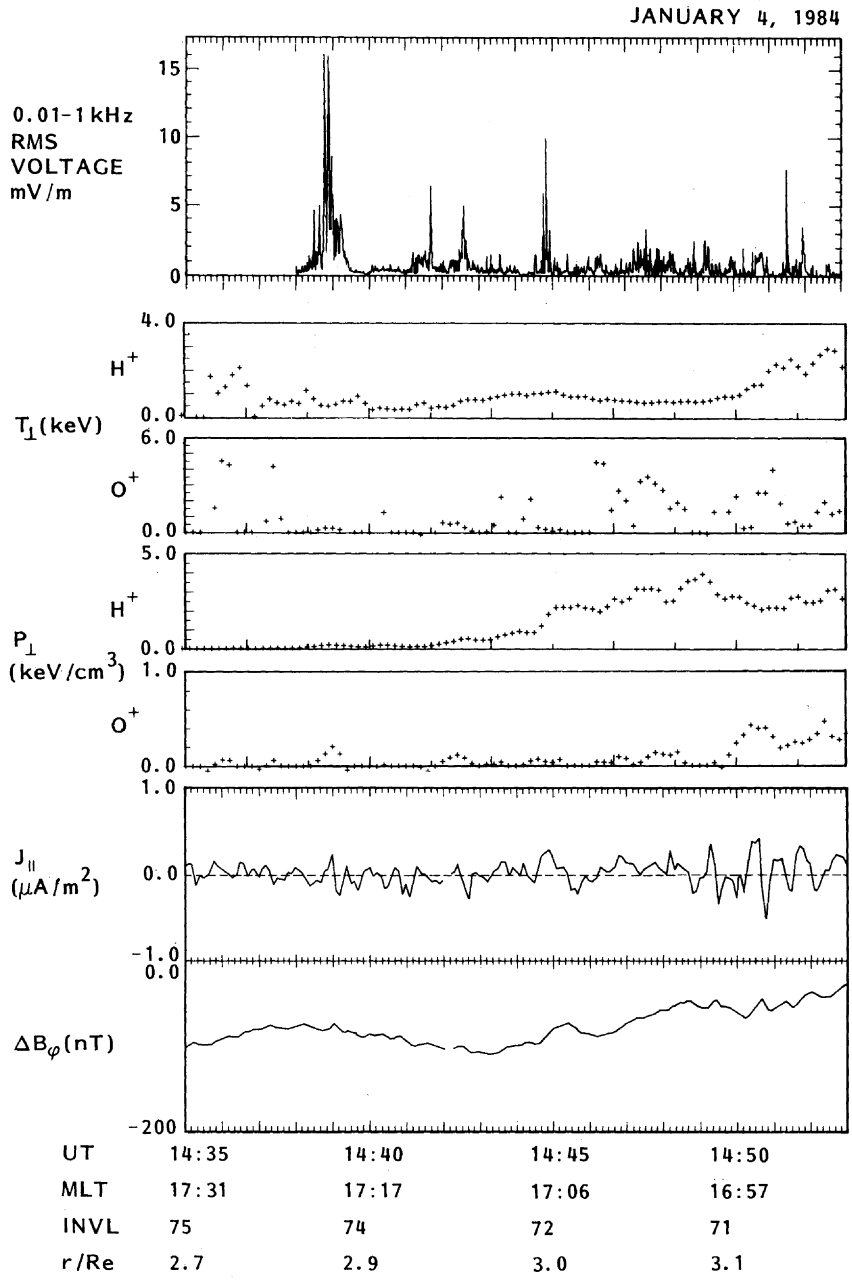

Fig. 2. Medium time resolution plasma parameters observed for part of the interval displayed in Figure 1. The top panel presents the observed root-mean-square (rms) voltage detected on the long-wire electric antenna in the frequency range 0.01 to 1 kHz. The second and third panels display partial ion temperatures in units of keV perpendicular to the magnetic field. The fourth and fifth panels present the partial ion pressure (perpendicular temperature times partial ion density) for hydrogen and oxygen in units of keV/cm^3. The bottom two panels present 6-s averages of data obtained from the high-resolution magnetometer. The bottom panel displays the difference between a model and the measured east-west component of the magnetic field in units of nanoteslas. The sixth panel displays the small- scale field-aligned currents in units of microamperes per square meter. These currents are obtained by differentiating the data in the lowest panel with respect to invariant latitude.

100-km level would be 15 to 20 times higher. The sixth panel of Figure 2 displays the small-scale field-aligned currents which are obtained by differentiating the data in the lowest panel with respect to invariant latitude. The most intense small-scale features with an indicated magnitude of greater than 0.2 μA/m^2 were detected near 1439, 1442:30, 1445 UT, and 1449, 1450:30, and 1452 UT.

As noted above, the thermal structure of the ion plasma normally encountered on auroral field lines is complex. The total plasma density as well as the relative contribution of the cool (less than $\sim$ 100 eV) and hot ion components changes rapidly during the interval presented in Figure 2. Plasma densities can be estimated from particle data, but these estimates are subject to considerable uncertainties. The most reliable method for determining plasma densities in the auroral zone available on the DE 1 satellite is to use the frequently observed "cutoff" in "auroral hiss" emissions at the electron plasma frequency (see, for example, *Persoon et al.*, [1983, 1988]). This frequency was well defined during most of the time interval displayed in Figure 2. Densities obtained from analysis of plasma wave features and associated uncertainties are indicated by the plus symbol, and error bars are presented in Figure 3. The smallest uncertainties reflect

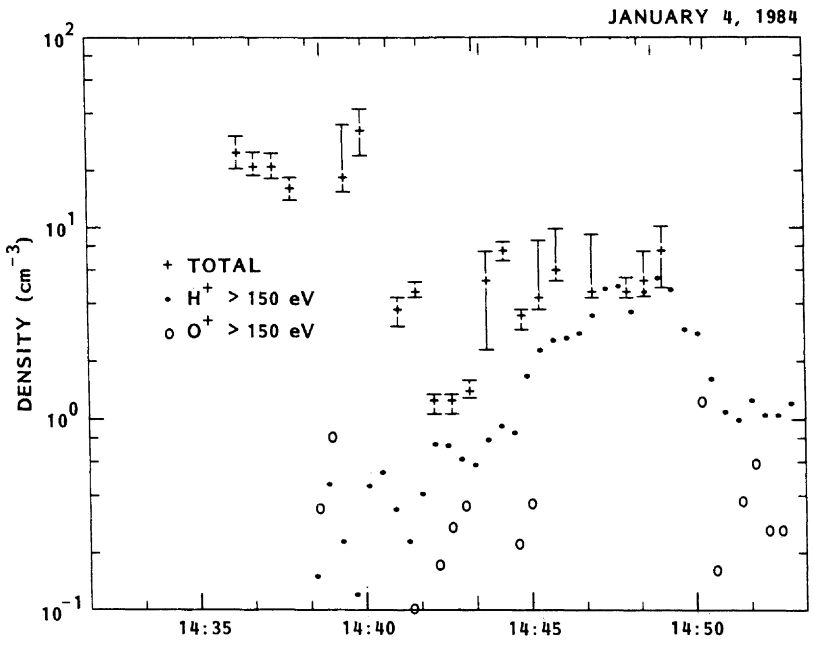

Fig. 3. Observed plasma densities for an interval on January 4, 1984. The total densities obtained from analysis of plasma wave features, and partial densities for hydrogen and oxygen ions with energies between 150 eV and 17 keV are shown.

the spacing between frequencies sampled by the swept frequency receiver; the largest uncertainties come from ambiguities in the cutoff frequency introduced by bursts of electrostatic noise propagating in the same frequency range as the auroral hiss and a noise band at 50 kHz (A. Persoon, private communication, 1987). The partial densities obtained from the lowest moment of EICS data over the energy range 150 eV to 17 keV for hydrogen and oxygen are indicated by the solid and open circles respectively. The absolute values of the partial EICS densities shown in Figure 3 were obtained using preflight calibration data and have uncertainties of approximately ± 30%, comparable to those displayed for the total density determined from the plasma wave instrument. The relative partial densities determined from the EICS (both in time and mass) are, however, quite well determined (i.e., on the order of a few percent). The plasma density profile of the auroral zone crossing displayed in Figure 3 is quite typical for the local time and altitude region (*Persoon et al.*, [1988]. The data in Figure 3 reveal strong gradients near 1440:30, 1442, and 1444 UT in the total density and near 1445, and 1451 UT in the partial energetic hydrogen density.

It is possible to estimate the contribution to the total density and relative composition of the thermal plasma (i.e., ions with energies less than 50 eV) from the retarding ion mass spectrometer (RIMS) instrument if the spacecraft potential is known. Unfortunately in the relatively low densities encountered on auroral field lines, the spacecraft potential can change rapidly, making routine density calculations of the thermal plasma difficult. A range of density values obtained by fitting the observed counting rates from the axial heads of the RIMS instrument for a range of satellite potentials and plasma drift velocities at selected times are given in Table 2. (Most of the times correspond to times of local maxima in the partial hydrogen perpendicular ion pressure displayed in Figure 2.) The range of thermal plasma densities shown in Table 2 is consistent with the relative contribution of the energetic plasma to the total density indicated in Figure 3. Furthermore, the densities and relative composition of the thermal plasma indicated in Table

TABLE 2. Total and Partial Plasma Densities for Selected Times

	Time, UT	Total Density, cm^{-3}		Thermal Plasma		Energetic Plasma > 150 eV	
				Composition H^+ / He^+ / O^+, percent	H^+ Density range, cm^{-3}	H^+	O^+
A	1438:56	18.36	+90 / -16%	98 / 2 / 0	0.9 – 10.0	0.46	0.8
B	1440:52	4.03	±18%	76 / 23 / 1	0.4	0.34	–
C	1442:33	1.32	±~12%	–	–	0.71	0.27
D	1443:39	5.36	+43 / -56%	90 / 9 / 1	0.1 – 0.3	0.78	–
E	1445:25	5.07	+66 / -12%	90 / 7 / 3	0.3 – 4.9	2.5	–
	1446:30	5	+100 / -7%	–	–	3.5	0.02
F	1447:39	4.61	+19 / -7%	91 / 5 / 4	0.3 – 0.4	4.9	0.05
G	1448:50	5.85	+35 / -36%	87 / 10 / 3	1.0 – 1.3	5.4	–
H	1450:20	5	–	–	0.4 – 5.0	2.0	1.3

The letters in the leftmost column refer to the labels in Figure 5.

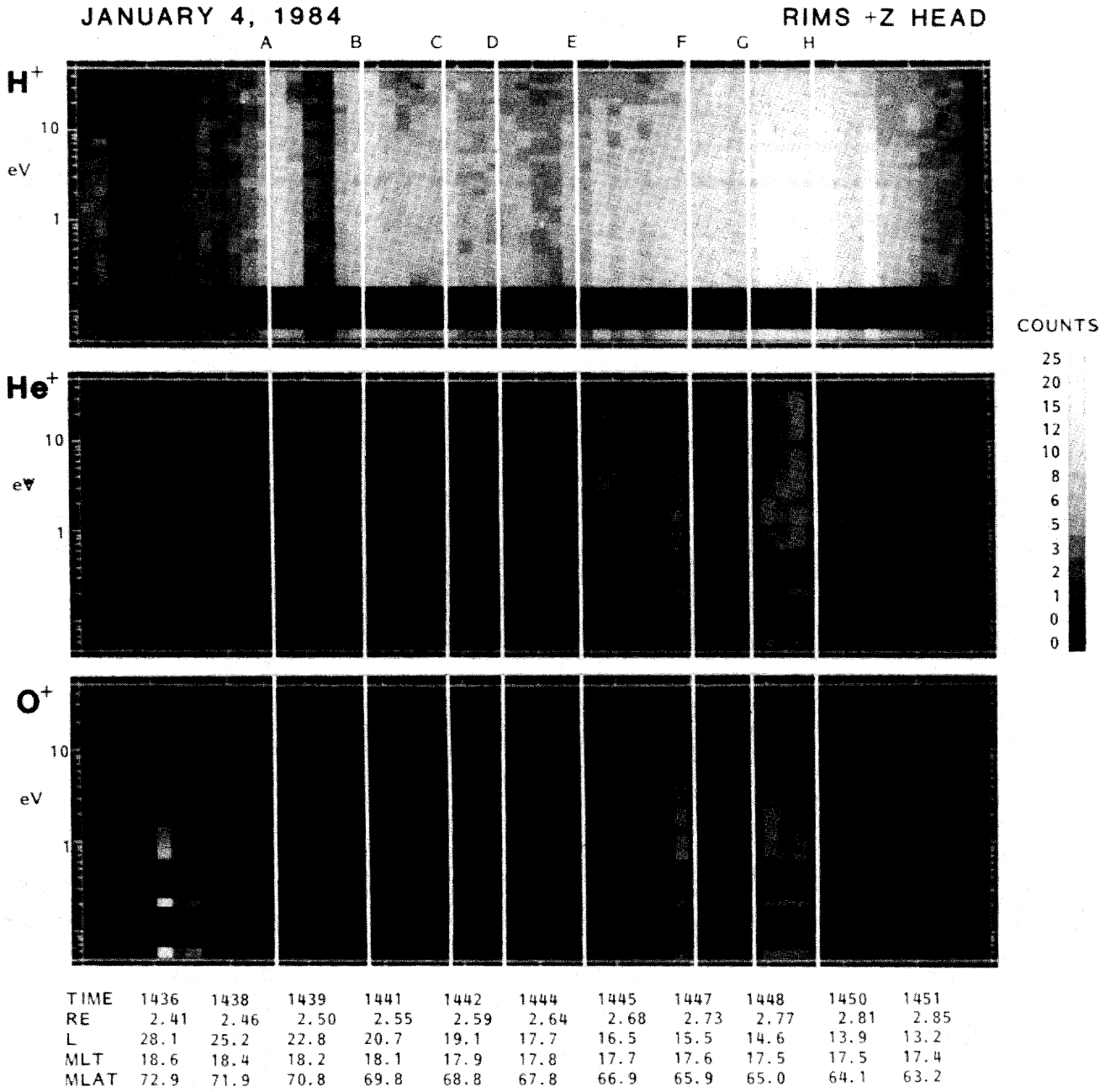

TIME	1436	1438	1439	1441	1442	1444	1445	1447	1448	1450	1451
RE	2.41	2.46	2.50	2.55	2.59	2.64	2.68	2.73	2.77	2.81	2.85
L	28.1	25.2	22.8	20.7	19.1	17.7	16.5	15.5	14.6	13.9	13.2
MLT	18.6	18.4	18.2	18.1	17.9	17.8	17.7	17.6	17.5	17.5	17.4
MLAT	72.9	71.9	70.8	69.8	68.8	67.8	66.9	65.9	65.0	64.1	63.2

Fig. 4. Thermal plasma transverse to the magnetic field direction detected by the retarding ion mass spectrometer (RIMS) instrument in energy-time spectrogram format. The count rate observed for hydrogen, singly charged helium, and oxygen, which is approximately proportional to the number flux of ions within the energy range of the RIMS instrument, is encoded using the gray bar on the right. The ordinate in each panel is the energy setting of the retarding potential analyzer from 0 to 50 eV. Vertical white lines labeled "A" through "H" have been drawn at the times indicated in Table 2. Note that time "ticks" indicated on the bottom are not located precisely at even minutes, but the time labels have been rounded to the nearest minute. The satellite position is indicated at the bottom.

2 are similar to those reported from other auroral zone intervals where the spacecraft potential was known or controlled [*Nagai et al.*, 1984; *Gallagher et al.*, 1986; and *Olsen et al.*, 1986]. and suggest that the thermal plasma is dominated by the polar wind.

The spatial structure of the thermal (less than 50 eV) ion plasma observed transverse to the magnetic field is illustrated in Figure 4. Hydrogen, singly charged helium, and oxygen energy spectra are encoded in an energy-time spectrogram format. The data are from one of the two RIMS sensors with a wide field of view that has its center look direction approximately transverse to the local magnetic field. The ordinate in each panel is the energy setting of the retarding potential analyzer from 0 (spacecraft potential) to 50 eV. The observed counting rate, which is approximately proportional to the number flux of ions within the energy range of the RIMS instrument, is encoded as a function of energy and time using the gray bar on the right. Average energy spectra for successive 18-s intervals are displayed. (Eighteen seconds are required to obtain complete energy, mass, and angle coverage

in the operational mode used.) Vertical white lines labeled "A" through "H" have been drawn at the times indicated in Table 2. Note that time "ticks" indicated on the bottom are not located precisely at even minutes, but the time labels have been rounded to the nearest minute. Where the thermal ion plasma dominates the density (i.e., before ~ 1442 UT) there are well-defined maxima in the fluxes of observed thermal plasma. After ~ 1442 UT where the thermal plasma is not dominant, we see indications of intensification and energization of hydrogen ions in the RIMS data presented in Figure 4.

As noted above, the plasma encountered on auroral field lines is a variable mixture of the ambient cold plasma and upflowing ionospheric plasma, as well as downflowing, precipitating, and mirroring hot plasma sheet plasmas. The data presented above demonstrate that on this auroral zone crossing, the thermal structure changes from predominantly cool (or polar wind like) before ~ 1440 UT to predominantly energetic (or plasma sheet like) after ~ 1444 UT. The increase in hydrogen partial perpendicular pressure seen in Figure 2 between ~ 1442 and 1449 UT reflects this transition and is not the result of local ion energization processes.

The low-frequency plasma wave emissions observed during the interval under consideration have so far been presented in summary form. High-resolution plasma wave spectrograms are presented in Figure 5. More intense emissions appear darker. The waveform was logarithmically compressed before transmission, and the spectrogram format has not been corrected for this compression. Regions of relatively intense low-frequency plasma wave emissions not apparent in Plate 1 or Figure 2 are easily identified. Multiple "bands" of intense low frequency emissions are seen from ~ 1446 to ~ 1449 UT, and there is a strong emission feature at several hundred hertz between ~ 1440 and ~ 1441 UT. Localized regions of low-frequency emissions extending to the lowest detectable frequencies are seen near 1439, 1442:30, 1445 UT, between 1441 and 1442 UT and intermittently at other times. To understand the nature of the plasma waves we need estimates of the local lower hybrid resonance and hydrogen gyrofrequencies. Densities and relative compositions, consistent with the particle observations and the calculated lower hybrid resonance frequency, which depends on the plasma density and weakly on ion composition, for several times of interest are presented in Table 3. Also shown in Table 3 are the observed magnetic field strength and hydrogen ion gyrofrequency. Examination of Table 3 shows that the banded plasma wave emission features seen in Figure 5 are at or below the local lower hybrid resonance frequency.

Line plots of wave spectra as a function of frequency observed at four times near 1439 and 1447 UT are presented in Figure 6. The vertical lines in Figure 6 have been drawn at multiples of the local hydrogen gyrofrequency determined from the magnitude of the measured magnetic field. The local hydrogen gyrofrequency changed from ~ 60 Hz near 1439 to ~ 45 Hz near 1447 UT. Near 1439 UT, the wave intensity peaks slightly above the first few harmonics of the local gyrofrequency for all local gyrofrequencies between 1438:30 and 1439:00 UT. Between 1446 and 1447 UT the hydrogen gyrofrequency changes from 45.3 to 42.4 Hz. The local hydrogen gyrofrequency at 1446:33 UT is 44.5 Hz, which places emission peaks slightly above the sixth through tenth harmonics. However, the data near 1447 UT are also consistent with the emission peaks occurring at multiples of 45 Hz. It is obvious from Figure 5 that no one plasma wave mode could be responsible for the variety of features seen.

During the interval 1430 to 1500 UT, the oxygen gyrofrequency varied between ~ 7 and 2 Hz. Emissions at these low-frequencies would not be detectable in data presented in the format of Figures 5 or 6 because of the Doppler broadening arising from the ~ 5-km/s satellite velocity. The digital data from the electric field portion of the plasma wave instrument were nevertheless examined for evidence of emissions below 8 Hz from 1425 to 1455 UT. No evidence for emission features at or spaced at the oxygen gyrofrequency was found. The PWI also provided a measurement of the component of large-scale plasma convection electric field in the spin plane of the satellite. The plasma convection normal to the orbit plane inferred from these measurements was predominately antisunward before 1439 UT and sunward after then. In the local time sector of the observations the sunward direction is approximately tangent to the auroral oval. Brief sunward convection intervals were observed at ~ 1435 and ~ 1438 UT, which is normal in this local time sector. The largest detected gradient in the perpendicular electric field (50 mV/m in about 30 s or 150 km near 1439 UT) was not strong enough to disrupt the ion gyromotion and thus heat the ions (see, for example, *Lysak* [1986]). The DC electric field is determined by fitting observed voltage levels for sequential spin periods (6 s). The scale size set by the 6 s averaging period, ~ 30 km, is large compared to the relevant ion gyroradii, which are less than ~ 1 km.

We are interested in the complex plasma interactions that occur on auroral field lines, and in particular those processes that lead to energization of ions transverse to the local magnetic field. We have adopted as a working criterion for identifying localized regions of transverse ion energization the simultaneous occurrence of intense low-frequency (less than ~ 1000 Hz) plasma waves and local maxima in either the perpendicular plasma pressure or temperature. Table 4 summarizes the relevant data presented in Figures 2 through 6. To study the connection, if any, between the low-frequency plasma waves and increases in partial perpendicular ion pressure or temperature presented above it is essential that both the particle and wave data are not temporally biased, i.e., there be no strong gradients in the plasma density and the low-frequency emission feature lasts for a few spin periods. The addition of this third criterion eliminates most of the intervals identified above. We limit further discussion to three intervals: two that satisfy all three selection criteria (near 1439, and 1442:30 UT); and a third (from ~ 1446 to ~ 1449 UT) because of the close association of an identifiable feature in the hydrogen ion velocity space distribution (presented below) with the observed banded plasma wave emissions seen at this time.

The Plasma Environment Near 1439 UT

This interval was selected because the local maxima in hydrogen and oxygen partial ion pressure (Figure 2) correspond with the center of a well-defined feature in the low-frequency plasma wave data (Figures 2 and 5). Near 1439 UT there are also an oppositely directed small-scale field-aligned current feature (Figure 2) and large-scale plasma convection reversal (not shown). The plasma composition is dominated by thermal hydrogen ions.

The electric field waveform for this interval appears to be quasi-coherent in nature with periodic waveforms lasting for about 5 periods. The peak to peak amplitude of this quasi-coherent wave is on the order of 10 mV/m as determined from a rectified waveform which is monitored and transmitted separately from the wideband signal. Because the waveform was logarithmically compressed and the spectrogram format of Figure 5 is not corrected for this compression, it is not apparent that most of the wave power is concentrated near the hydrogen cyclotron frequency and that there is

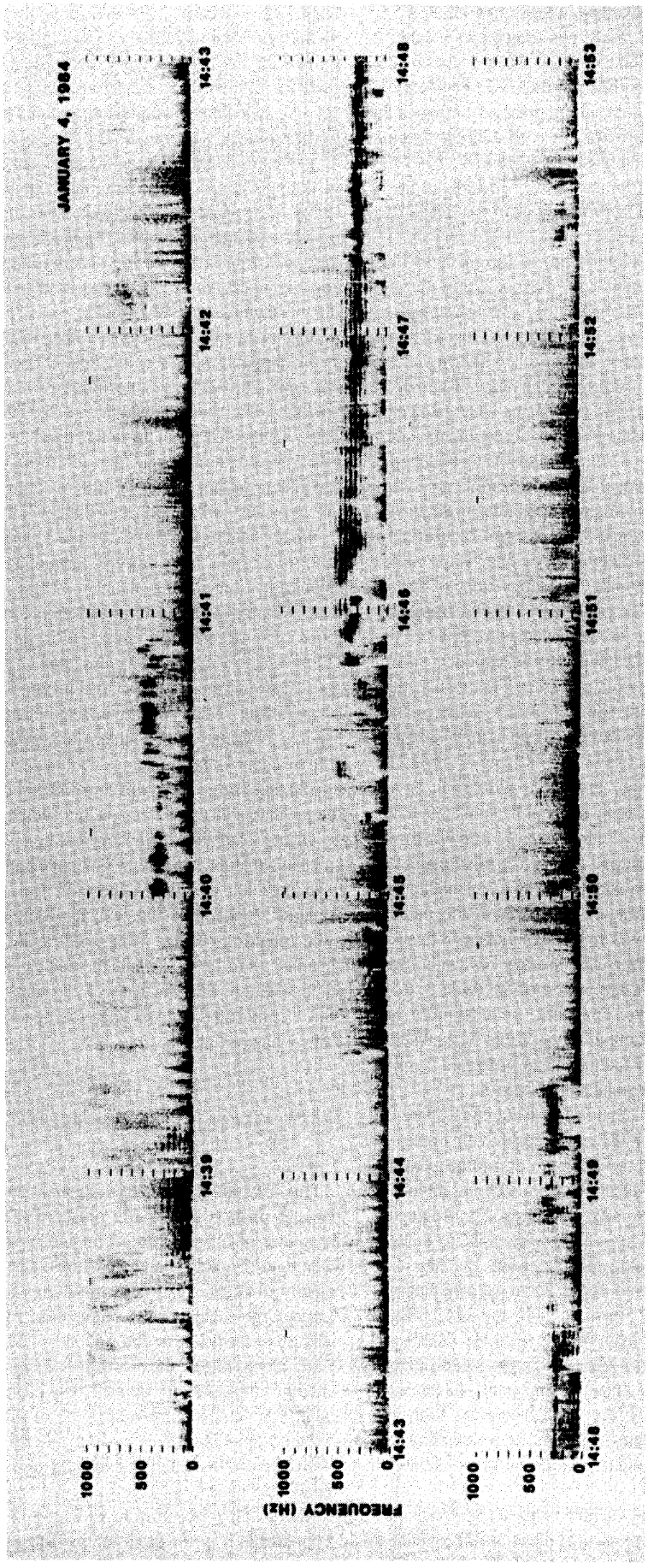

Fig. 5. Plasma wave spectrograms obtained from the wide-band receiver observed from 1438 to 1453 UT displayed in frequency-time spectrogram format. Data are available for the range 0.01 to 10 kHz, but only the range 0.01–1 kHz is displayed. More intense emissions appear darker. The waveform was logarithmically compressed before transmission, and the spectrogram format has not been corrected for this compression.

TABLE 3. Estimates of the Lower Hybrid Resonance Frequency for the Selected Times

	Time, UT	Strength of Magnetic Field, gauss	Hydrogen Gyrofrequency, Hz	Composition estimates (Density, cm^{-3})			Lower Hybrid Frequency, Hz
				H^+	He^+	O^+	
A	1438:56	0.039	60	18.4	–	–	850
				11.0	7.4	–	711
				11	7.0	0.4	709
				10	7	1.4	682
				35	–	–	1116
				20	13	2	913
B	1440:52	0.036	55	4.0	–	–	416
				2	1	1	318
				2	2	–	330
				3.3	–	–	380
				2.3	0.5	0.5	329
C	1442:33	0.034	52	1.3	–	–	243
				1	0.15	0.15	219
				1	–	–	216
D	1443:39	0.033	50	5.4	–	–	478
				4.9	0.5	–	461
				4.8	0.5	0.1	457
E	1445:25	0.030	46	5	–	–	458
				4.5	0.5	–	441
				4	0.5	0.5	418
				8.4	–	–	581
				7.0	0.7	0.7	540
	1446:30	0.030	46	5	–	–	458
				4.4	0.5	0.1	436
				4	0.5	0.5	418
				10	–	–	630
				8	1	1	574
F	1447:39	0.028	43	4.6	–	–	439
				4.2	0.4	–	424
				4.1	0.4	0.1	419
				3.8	0.4	0.4	405
G	1448:50	0.027	41	5.85	–	–	489
				5.25	0.5	0.1	469
				5.65	0.1	0.1	482
				5.75	0.1	–	486
				3.74	–	–	397
H	1452:20	0.026	40	5.5	–	–	474
				5.0	0.5	–	457
				4.9	0.5	0.1	453
				4.9	0.1	0.5	450

The labels A–H refer to features marked in Figure 5.

a significant spin modulation of the received signal. The maximum electric field intensity occurs roughly perpendicular to the magnetic field lines. Based on measurements of only one component in the spin plane, we estimate that the ratio of parallel to perpendicular wave number is 0.20 ± 0.16. The digital magnetic field values from the low-frequency correlator (LFC) of the PWI instrument show an enhancement in the less than 100 Hz magnetic field components centered around the event. This magnetic component of the waveform could be produced by the motion of the satellite through a filamentary current region or could be related to the saucer feature seen from ~ 1438:20 to ~ 1439:20 UT.

The plasma waves observed near 1439 UT appear to be electrostatic ion cyclotron waves. The evidence for this is that (1) the emissions peak at frequencies slightly above the hydrogen cyclotron frequency and (2) the emissions are centered on a time corresponding to a pair of field-aligned currents with magnitudes $\sim 2 \times 10^{-7}$ A/m^2. The possibility that the plasma waves near 1439 UT are Alfven waves can be ruled out for the following reasons: (1) The fundamental frequency is slightly above the hydrogen cyclotron frequency. (For an Alfven wave the fundamental frequency has to be below the H^+ cyclotron frequency.) (2) The possibility of a Doppler-shifted Alfven wave can be ruled out because the Alfven velocity, ~ 10^5 km/s, is much greater than the satellite velocity, ~ 5 km/s. (3) The index of refraction computed from the ratio of electric and magnetic power spectral densities (0.82) does not agree with the Alfven index of refraction computed from the local plasma mass density and magnetic field strength (~ 32). The saucer feature noted above is the most likely source of the weak, low-frequency, magnetic power detected near 1439 UT. We cannot, however, completely rule out the possibility that the waves are whistler mode emissions, some modes of which can propagate below the lower hybrid frequency.

If the wave emission features observed near 1439 UT are electrostatic ion cyclotron waves, we can then evaluate the possibility that the observed field- aligned current at this time is the source of free energy driving these plasma waves. *Kindel and Kennel* [1971] noted that emissions near multiples of the hydrogen gyrofrequency could be excited when the drift velocity of ionospheric electrons carrying a field-aligned current exceeded some fraction of the electron thermal velocity.

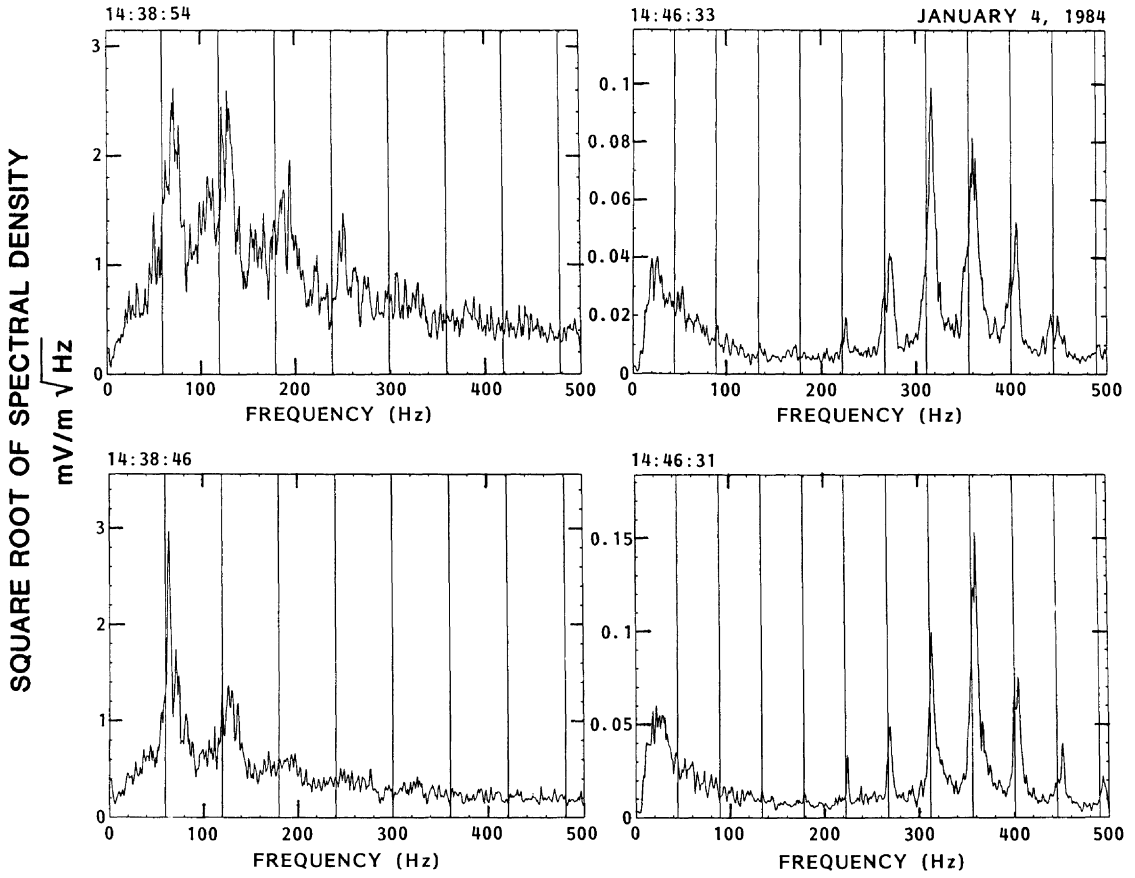

Fig. 6. Line plots of wave spectra as a function of frequency observed at four times near 1439 and 1447 UT. The vertical lines are at multiples of the local hydrogen gyrofrequency determined from the measured magnetic field at the time the spectrum was acquired.

$$J_c > F\,N\,V_{eth} \quad (1)$$

where F is the fraction (between 0.1 and 1.0), N is the local plasma density, and V_{eth} is the thermal velocity of the electrons carrying the field-aligned current. J_c is the field-aligned current in the appropriate units of velocity and density. This relation can be recast and a velocity calculated from the observed current and density which can be used to determine electron thermal speeds (or energies) below which the *Kindel and Kennel* [1971] criteria for producing a current-driven instability are met. Table 5 presents electron thermal energies in electron volts and degrees Kelvin for a range of densities and the fractional parameter F consistent with data in Figure 2 and Table 2. To use Table 5, we must estimate the local electron temperature.

Electron temperatures have not been systematically measured at these high altitudes, so we must rely on the guidance of infrequent measurements and ionospheric models of electron thermal velocities. *Kintner et al.*, [1978] inferred an electron temperature of 3.4 eV (39,000 K) in a region with plasma wave and ion data at $r/R_E \sim 2$ similar to that reported here at $r/R_E \sim 3$. Models such as the one recently presented by *Mitchell and Palmadesso* [1983] suggest a very weak falloff of electron temperature with altitude above $r/R_E \sim 2$. The model of *Mitchell and Palmadesso* [1983], however, suggests a much lower ambient electron temperature of a few thousand degrees Kelvin or ($\sim$ 0.1 eV) at these altitudes. The critical electron temperatures reported in Table 5 for 1439 UT are generally well below the 3.4-eV value inferred from the S3-3 data but above the theoretical value of 0.1 eV. Our imprecise knowledge of the local electron temperature and plasma density then does not allow us to use relation (1) above to evaluate the importance of field-aligned currents in the plasma heating observed near 1439 UT.

If the plasma waves seen near 1439 UT were the result of a local current-driven instability, then we could expect some evidence of enhanced ion fluxes perpendicular to the local magnetic field, the so-called 90° pitch angle ion conic signature. As noted by *Peterson et al.*, [1986] and shown below, the hydrogen and oxygen fluxes observed by both DE ion mass spectrometers peak at angles between 180° (field aligned) and 90°. A simple calculation based on a dipole magnetic field model and conservation of the first adiabatic invariant shows that these ions would have had 90° pitch angles within 1000 km below the satellite, well above the ionosphere. It should also be noted that there could in fact be a minor (i.e., on the order of a few percent) component of the observed ion distribution that does in fact peak at 90° in pitch angle but is masked by the larger population flowing up the magnetic field.

The waveform indicates that the high-intensity plasma waves are not occurring continuously throughout the event but intermittently. If the waves are electrostatic hydrogen cyclotron waves caused by a current-driven instability, the discussion above suggests that the thermal electron component which drives the instability is filamentary. This filamentary current would not show up in the magnetometer data.

There are several sources of energy, other than the current-

TABLE 4. Summary of Identifiers of Transverse Ion Energization

Time, UT	Local Maxima in Partial Ion Pressure		Local Maxima in Partial Ion Temperature		Intensification of Thermal Plasma			Low Frequency Plasma Wave Emissions	Field Aligned Currents	Plasma Density Gradients
	H^+	O^+	H^+	O^+	H^+	O^+	He^+			
1439 (A)	X	X	–	X	X	X	–	X	X	–
1440:30 (B)	X	–	–	–	X	–	–	*	–	X
1441:30	–	–	?	–	–	X	–	X	–	–
1442:30 (C)	X	X	–	X	?	–	–	X	X	–
1444 (D)	X	–	–	–	?	–	–	–	–	X
1445	–	–	–	–	–	–	–	X	X	X
1445:30 (E)	X	–	–	–	?	–	–	–	–	–
1447:30 (F)	X	–	–	X	X	X	X	**	–	–
1449 (G)	X	–	–	–	–	–	–	**	?	–
1450 (H)	?	–	–	?	–	–	–	–	–	X
1450:30	–	X	?	–	–	–	–	–	X	X
1451:30	?	–	X	–	–	–	–	X	X	X
1452:30	?	–	X	–	–	–	–	X	X	X

The times indicated by A through H refer to times indicated on Figure 5. The last intensification of low-energy ions occurs near 1451 UT. Symbols are as follows: X, the indicated plasma or plasma wave condition was observed; ?, the indicated plasma or plasma wave condition may have been observed; *, from 1440 to 1441 UT there was an intense emission near the lower hybrid resonance frequency; and **, from 1446 to 1449 UT intense banded emissions near and below the lower hybrid resonance frequency were detected.

driven instability, that could cause the plasma waves observed near 1439 UT. For example, low-energy upflowing ion beams or the locally intense fluxes of ions transverse to the magnetic field could provide this energy (see, for example, *Bergmann* [1984], *Kaufmann and Kintner* [1982], *Kintner* [1980], and *Andre et al.* [1986]). Some of these sources of energy are in fact present, as can be seen by examining detailed ion measurements obtained from 1438 to 1440 UT which are presented in Figures 7, 8, and 9 and discussed below.

The velocity space density contour plots presented in Figure 7 retain the full temporal resolution of the EICS instrument; each frame presents the data from one 6-s satellite spin period. The EICS instrument was operating in a mode that had a four-spin (24-s) period. In this mode, oxygen and hydrogen were sampled during alternate 6-s spin periods, and two different interleaved energy spectra were sampled 24 times per spin for two spin periods each. The lowest-energy channel used in this mode, which is sensitive to ions with energies from 10 eV to ~ 125 eV, is sampled for only two of the four spins in the cycle. The contours shown in Figure 7 are of the common logarithm of velocity phase space density measured in the satellite spin plane in a coordinate system aligned with the local magnetic field and are spaced at half-decade intervals. Velocities parallel to the local magnetic field are displayed on the horizontal axis. Ions flowing up the field line have negative parallel velocities. The positions in velocity space of the center energies of each measurement are indicated by dots. The velocities (energies) displayed have been corrected for the ~ 5-km/s spacecraft velocity. The surface contoured is defined by the larger of the one-count instrumental response or the actual measurement at each sample point; thus the full circles and large arcs centered near the origin are contours of the one-count-per-sample surface. Complete circles in the oxygen contour plots for the intervals starting at 1438:15 and 1439:27 UT show that the EICS instrument did not detect any oxygen ions for these 6-s periods. The increase in oxygen partial perpendicular pressure near 1439 UT (Figure 2) is clearly visible as an increase in the extent of the oxygen contours perpendicular to the magnetic field for the spin periods beginning at 1438:51 and 1439:03 UT. The increase in the hydrogen partial perpendicular pressure at this time is not immediately visible in the two-dimensional contours of Figure 7, but it is easily seen in one- dimensional velocity space distributions as a function of energy perpendicular to the magnetic field. Figure 8 presents one-dimensional velocity distributions for four of the 6-s hydrogen sampling intervals shown in Figure 7, and a curve representing the one-count per sample level of the EICS instrument. The labeled curves plotted in Figure 8 were obtained by integrating the surfaces presented in Figure 7 over the parallel velocity component. The unlabeled solid curve in Figure 8 represents the one-count per sample level of the EICS instrument similarly integrated. The distribution functions during the spin periods starting at 1438:51 and 1439:09 UT show significant increases in the number of hydrogen ions with energies above a few hundred electron volts perpendicular to the magnetic field. The spin period starting at 1439:09 UT also has almost 10 times as many hydrogen ions with perpendicular energies of ~ 200 eV than those periods starting at 1438:21 or 1439:33 UT, outside the region of intense wave emissions shown in Figures 2 and 5. Fig-

Table 5. Threshold electron thermal energy for stability inferred from Equation (1) for reasonable values of density N and fraction F using data for the times indicated

N, cm^{-3}	$F = 0.1$	$F = 0.5$	$F = 1.0$
	January 4, 1984 1439 UT		
35.0	0.78/ 9,050	0.03/ 348	0.01/ 116
18.4	2.9 / 33,600	0.11/ 1,280	0.03/ 348
15.0	4.3 / 49,900	0.17/ 1,970	0.04/ 464
	January 4, 1984 1442:30 UT		
1.5	430.0 /4,990,000	17.0 /197,000	4.0 /46,400
1.32	550.0 /6,380,000	22.0 /255,000	5.5 /63,800
1.1	790.0 /9,160,000	32.0 /371,000	7.9 /91,600
	January 4, 1984 1446 to 1449 UT		
5.0	9.6 / 111,000	0.4 / 4,640	0.1 / 1,160
7.0	5.0 / 58,000	0.2 / 2,320	0.05/ 580
10.0	2.5 / 29,000	0.1 / 1,160	0.02/ 232

The energies reported are in the units of electron volts / degrees Kelvin. If the in situ electron temperature is higher than the value reported here, the criterion in equation (1) for the current driven instability is not met for the specified values of N and F.

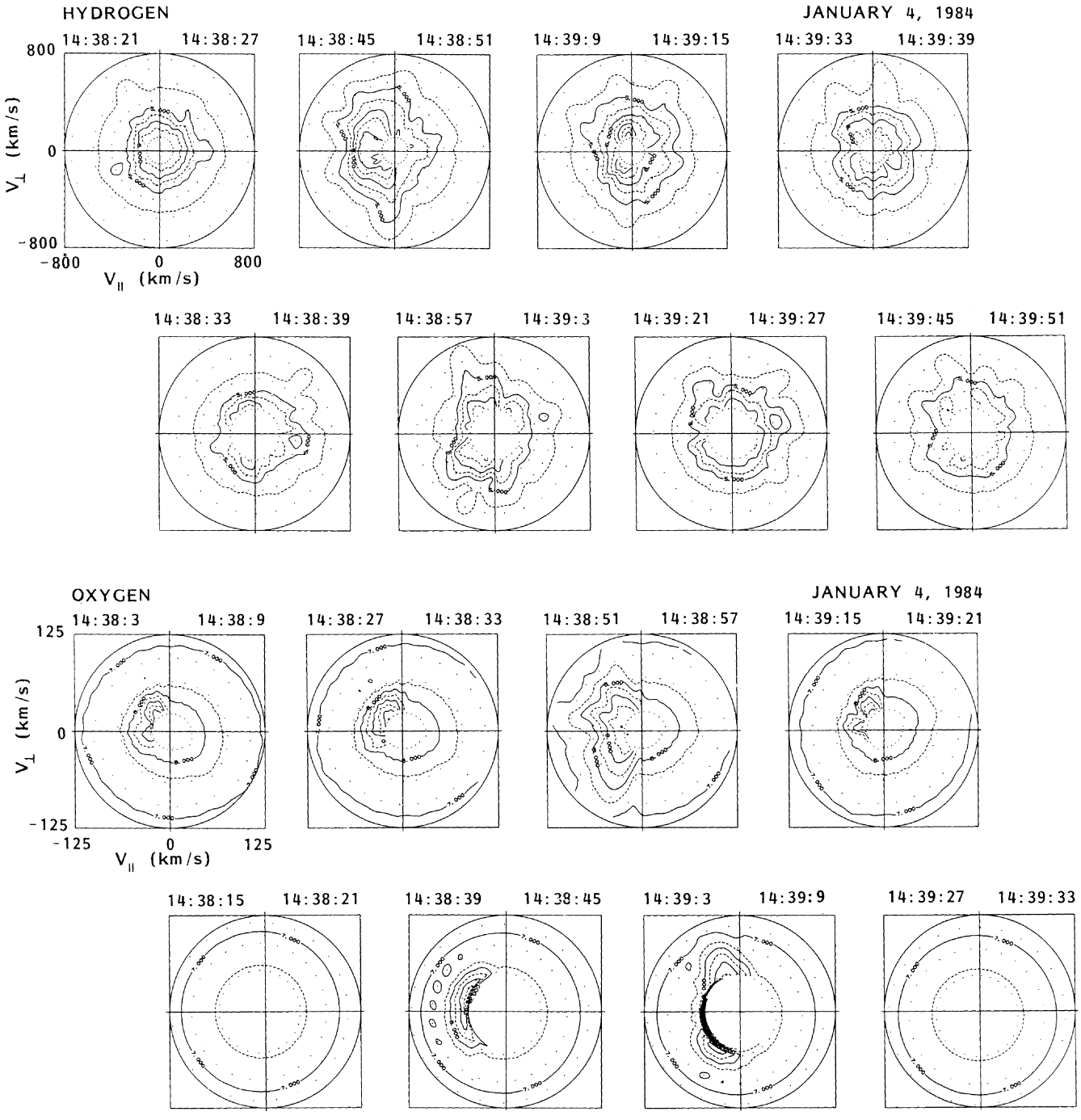

Fig. 7. Velocity space density contour plots which retain the full temporal resolution of the EICS instrument. The contours are of the common logarithm of velocity phase space density in units of s^3/km^6 measured in the satellite spin plane in a coordinate system aligned with the local magnetic field. The contours are spaced at half- decade intervals. Velocities parallel to the local magnetic field are displayed on the horizontal axis. The surface contoured is defined by the larger of the one-count instrumental response or the actual measurement at each sample point. Full scale hydrogen and oxygen velocities are 800 and 125 km/s respectively.

ures 7 and 8 thus show that there are locally intense fluxes of transverse ions which could provide the free energy to drive the plasma waves observed near 1439 UT.

The detailed oxygen ion distributions shown in Figure 7 suggest the existence of a low-energy upflowing beam before and after the interval between 1438:51 and 1439:09 UT where, as noted above, there is a substantial increase in the oxygen ion energy perpendicular to the local magnetic field. In fact the oxygen distribution is not beam-like after ~ 1438 UT. This can be seen in the RIMS radial head data shown in Figure 9 which are presented in angle-time spectrogram format. H^+, He^+ and O^+ ions detected by the RIMS instrument, independent of their energy, are displayed as a function of the instrumental look direction. The satellite velocity or ram direction is zero degrees (i.e., the middle of each panel) in the format of Figure 9. If the low-energy ions were stationary in the plasma frame of reference, they would appear in the ram di-

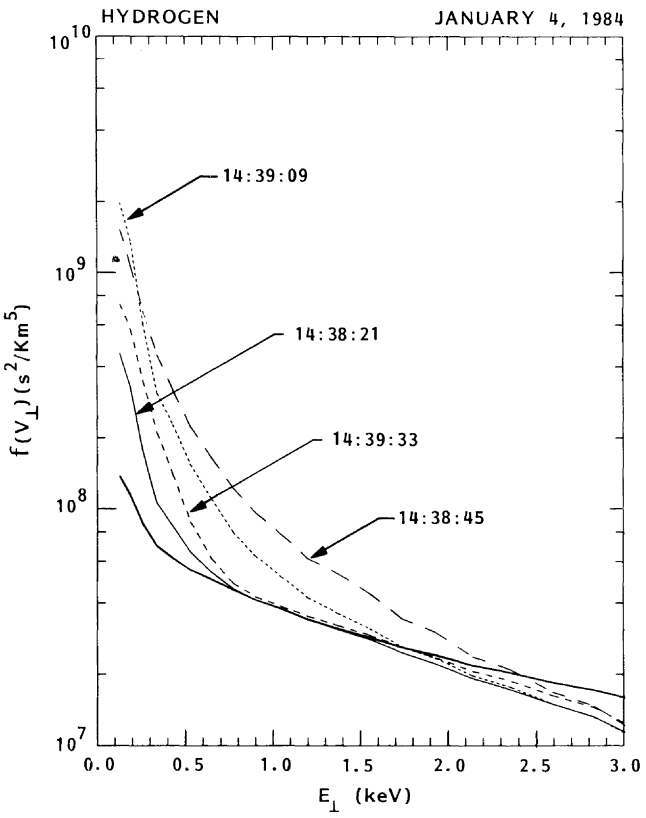

Fig. 8. One-dimensional hydrogen velocity space density distributions for four of the 6-s hydrogen sampling intervals shown in Figure 7, and a curve representing the one-count per sample level of the EICS instrument (heavy solid line).

rection. The two horizontal white lines in each panel indicate the directions of the local magnetic field. Low-energy ions flowing up the magnetic field line from the ionosphere below will appear near the magnetic field direction indicated by the solid white lines. Four vertical markers near the 1439 UT event at the times 1438:03, 1438:27, 1438:51, and 1439:15 UT have been added to Figure 9 to aid in identifying the feature near 1439 UT in the RIMS data. (Note that the time "ticks" indicated on the bottom of Figure 9 are not located precisely at even minutes, but the time labels have been rounded to the nearest minute.) The upflowing low-energy oxygen distribution is in fact beam like before 1438 UT, but it can be characterized as a simple beam after this time. Figure 9 also shows that the hydrogen and singly charged helium ion distributions observed near 1439 UT have conic type angular distributions that do not peak at pitch angles of 90°.

Since the observed ion distributions near 1439 UT are not beamlike, we can rule out upflowing ion beams as the source of free energy driving the low-frequency plasma waves. We now consider if the intense plasma waves seen near 1439 UT could be driven by the local ion conic distributions. It is possible that the extra flux of ions transverse to the local magnetic field could have been generated some distance below the satellite and are in fact the source of free energy for the low-frequency plasma emissions near 1439 UT (see, for example, *Andre et al.* [1986]). Clearly there are significant fluxes of energetic oxygen and hydrogen, and perhaps singly charged helium, ions with large velocities perpendicular to the local magnetic field, and their distribution has a local maximum near 1439 UT. The event was in fact selected because of their presence in the greater than 150 eV EICS data presented in Figure 2. Figures 7, 8, and 9 show that transversely energized ions are present even below 150 eV. We have presented evidence above that suggests that the extra flux of ions transverse to the local magnetic field observed near 1439 UT do not appear to be the result of a local current-driven plasma instability.

The velocity space distributions shown in Figure 7 are, within the limits of the measurement, similar to oxygen ion distributions presented by *Klumpar et al.* [1984] and *Chang et al.* [1986]. These authors have interpreted their observations in terms of a nonlocal acceleration process acting over extended altitude regions. Unfortunately, the low energy of the oxygen distribution presented in Figure 7 and the broad energy width of the lowest EICS energy channel (10 eV to ~ 125 eV) make it difficult to resolve details of the distribution below 125 eV and test the data in terms of the interpretations put forth by *Klumpar et al.* [1984] and *Chang et al.* [1986].

To summarize our observations of the plasma environment near 1439 UT, we have shown that the significant increases in hydrogen and perhaps oxygen ions with energies of several hundred volts perpendicular to the magnetic field seen near 1439 UT could be (1) the result of heating or energization of the plasma up to 1000 km below the spacecraft, and these perpendicular ions could be the source of the free energy creating the observed plasma waves; or (2) if the waves are electrostatic hydrogen cyclotron waves caused by a current-driven instability, the flux of cold thermal electrons that drive the instability is filamentary. We found no evidence for the existence of upward flowing ion beams at this time, and we noted that the observed low-energy oxygen distributions are, within observational uncertainties, similar to those recently reported by *Klumpar et al.* [1984] and *Chang et al.* [1986] and interpreted in terms of transverse acceleration mechanism operating over an extended altitude range.

The Plasma Environment Near 1442:30 UT

The low-frequency plasma waves observed near 1442:30 UT, in some respects, are similar to those observed near 1439 UT. In particular the observed wave intensity is maximum at the lowest frequencies, and the maximum electric field component generally occurs almost perpendicular to the magnetic field. The average rms electric field intensity integrated over the 0.01- to 1-kHz band is on the order of 3 mV/m. Typical values for the index of refraction computed from the ratio of electric and magnetic power spectral densities for this observation are 0.1 to 20, but the index could be much higher since the magnetic field values are at the instrument noise level. The emissions near 1442:30 UT are also associated with a pair of field-aligned currents of ~ 2×10^{-7} A/m^2. The waveform near 1442:30 UT, however, shows no harmonic structure, and there are no detectable coherent features.

If the plasma waves observed near 1442:30 UT are electrostatic, Table 5 shows that the low plasma densities make it much more probable that the *Kindel and Kennel* [1971] criterion for a current-driven plasma instability is met locally. Detailed distribution functions from the EICS instrument for spin periods near 1442:30 UT as presented in Figure 10 do not show a clear signature of 90° conics in either hydrogen or oxygen. (Note that the velocity scales used in Figure 10 are different than those used in Figure 7.) The RIMS radial head data for oxygen and hydrogen in Figure 9 also do not indicate ion fluxes with angular distributions peaking at pitch angles near 90°. The RIMS hydrogen and singly charged helium ion distributions near 1442:30 UT appear to be field aligned, while the oxygen distribution is of the conic

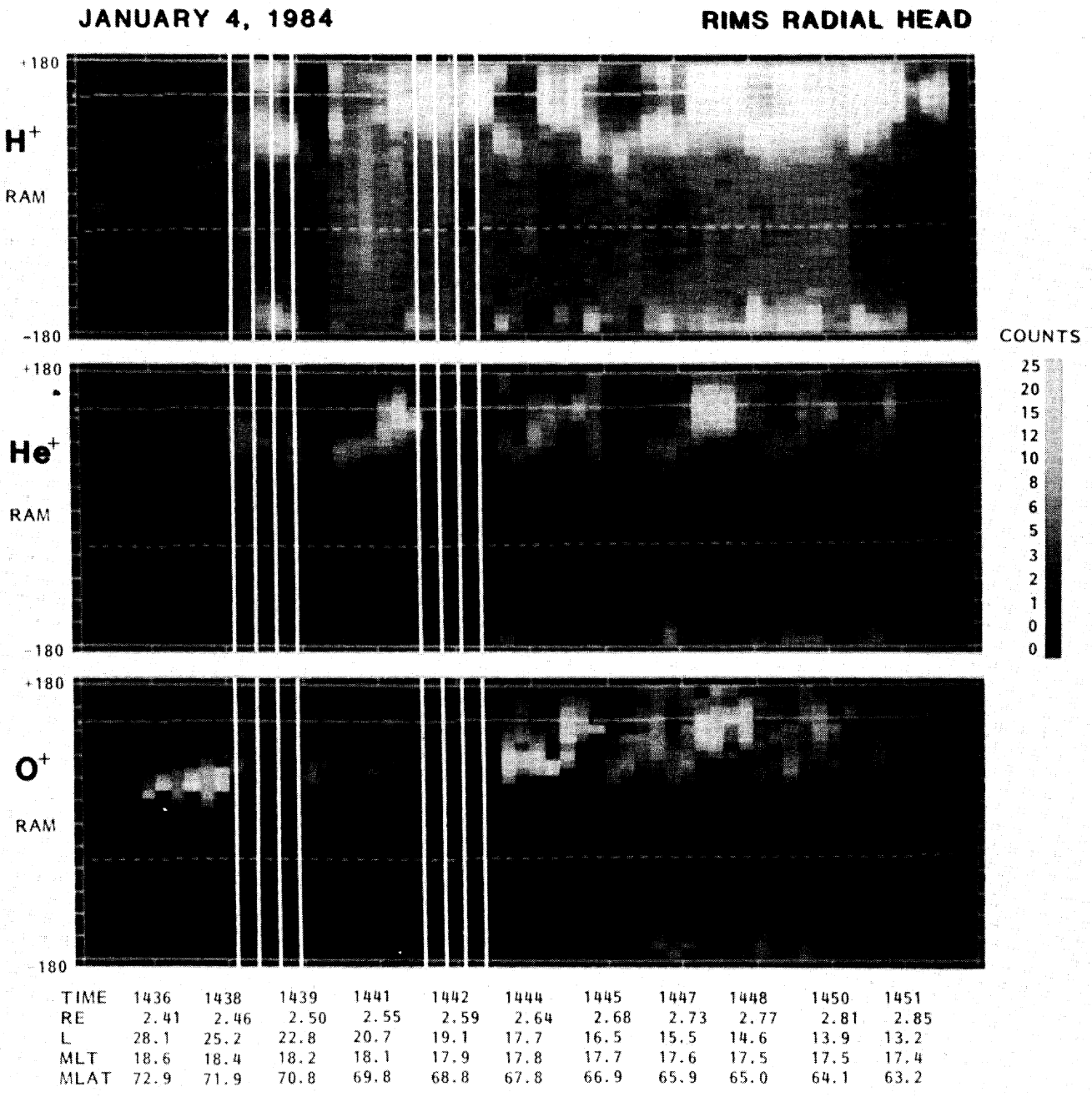

Fig. 9. Upflowing hydrogen, singly charged helium, and oxygen ions observed by the RIMS instrument in angle-time spectrogram format. The count rate, which is approximately proportional to the number flux of ions within the energy range of the RIMS instrument, is encoded using the gray bar on the right. The satellite velocity or ram direction is in the middle of each panel. The horizontal white lines in each panel indicate the directions of the local magnetic field. The vertical markers are at specific times identified in the text. Note that the time "ticks" indicated on the bottom are not located precisely at even minutes, and the time labels have been rounded to the nearest minute.

type. The low plasma density at this time introduces two further complications not present in the higher density plasma near 1439 UT. First, it is possible that the spacecraft has charged positively in the lower density environment and local transversely heated ions would not have enough energy to overcome this potential barrier. Second, there are simply not as many thermal hydrogen ions to heat or energize at this location (Table 3). There is also an instrumental threshold below which it is impossible to positively identify a small extra perpendicular component in the hydrogen distribution centered on 90° pitch angles at 1442:30 UT. We can therefore not exclude the possibility of a current-driven plasma instability occurring near 1442:30 UT.

The oxygen data centered on 1442:30 UT displayed in Figures 9 and 10 show that oxygen ions have an angular distribution similar to that observed near 1439 UT but are slightly more energetic. In summary, the event centered at 1442:30 UT has a particle and wave environment very similar to that observed near 1439 UT; the main differences are that near 1442:30 UT the plasma density is almost an order of magnitude lower and the plasma wave emissions are weaker.

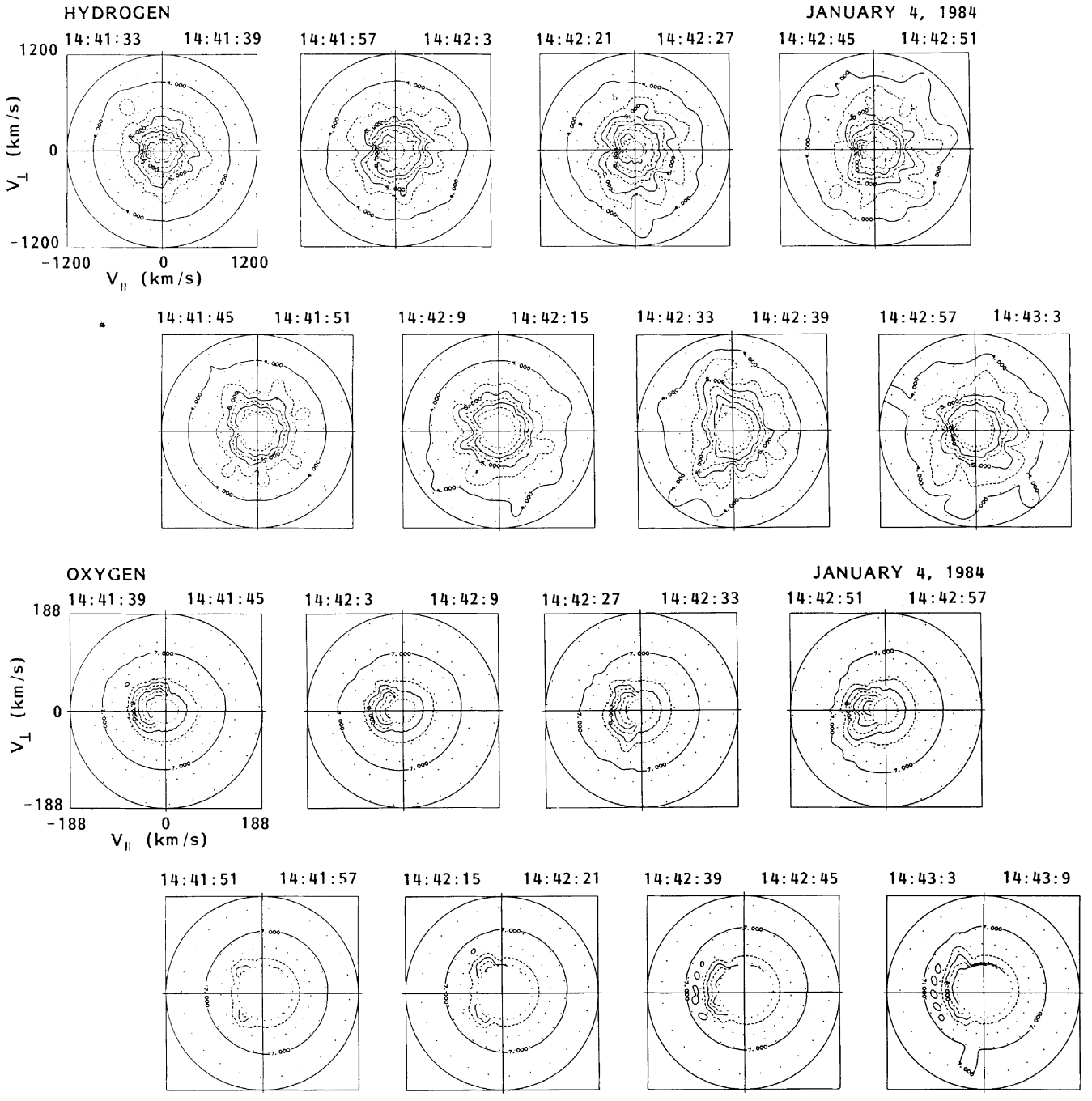

Fig. 10. Velocity space density contour plots for the time indicated in a format similar to that used in Figure 7. Note that here the full scale velocities of hydrogen and oxygen are 1200 and 188 km/s respectively.

The Plasma Environment From 1446 to 1449 UT

We have elected to present high-resolution particle and wave measurements from this interval because of the close association of an identifiable feature in the hydrogen ion velocity space distribution with observed banded plasma wave emissions. The strong banded plasma wave emission feature shown in Figure 6 from ~ 1446 to ~ 1449 UT does not correlate with a local maximum in the partial plasma pressure perpendicular to the magnetic field. There is a local maximum in partial perpendicular pressure at 1447:39 UT, but the emission feature extends beyond the two adjacent local minima shown at 1446:18 and 1448:08 UT in Figure 2. Before presenting and discussing the ion velocity space distribution feature we first present and discuss the high-resolution plasma wave observations.

The electric field waveform for this interval has periods where the waveform is highly coherent (i.e., there are intervals where as many as 30 wave periods can be identified). The frequency of these repeating waveforms is near 460 Hz (near the local lower hybrid resonance frequency shown in Table 3) and has an amplitude of approximately 1 mV/m. The high coherence and the narrow spectral widths suggest that the spectra are not due to bite-outs or absorption of auroral hiss. We have noted above, in the discussion of Figure 6, that the exact location of the emission peaks relative to harmonics of the hydrogen gyrofrequency

is uncertain because of the nonzero line widths and variation in the local magnetic field strength during this interval. The signal from the magnetic antenna is at the receiver noise level. Values of the index of refraction calculated from the ratio of measured electric and magnetic power spectral densities range from 0.2 to 10. The electric field intensity is strongly spin modulated with a maximum in intensity occurring roughly perpendicular to the field lines.

The RIMS data presented in Figure 9 show that there may be some transverse ion energization associated with these plasma waves, but this event is interesting because its long duration and relatively stable plasma conditions provide a very good opportunity to look for sources of free energy supporting the low-frequency wave emission feature. If these waves are generated in the region of the spacecraft, it should be possible to find a feature in the particle or magnetometer data and evaluate the free energy that could be derived from it. In fact two possible sources of free energy that could drive the plasma wave emissions have been identified: a field-aligned current or a shell-shaped downflowing hydrogen ion distribution. We will discuss each source in turn.

It is possible but improbable that the observed large-scale field-aligned current is the source of plasma waves under discussion. The possibility cannot be ruled out on the basis of in-situ plasma measurements. The magnetometer data presented in Figure 2 show a weak, upward directed field-aligned current in the range 0.5 to 2 $\mu A/m^2$ for the period 1446 to 1449 UT. Such currents can be carried by thermal electrons or energetic electrons precipitating into the atmosphere. The location of the satellite at 11,000 km, near the upper limit of the expected auroral parallel acceleration region, suggests that there are no local precipitating energetic electrons and that thermal electrons are the current carriers. If thermal electrons are carrying the observed current, then we can use relation (1) above to see if a current-driven plasma instability could be generating the observed plasma waves. Table 5 presents threshold electron thermal energies in electron volts and degrees Kelvin for a current of 1 $\mu A/m^2$, a range of densities consistent with the plasma measurements and the fractional parameter F described above. Since it is possible that the unmeasured local electron thermal energy could be lower than some of the values shown in Table 5, the plasma waves seen at this time could be the result of a current-driven instability. Detailed examination of both the hydrogen and oxygen ion distributions does not reveal ion angular distributions peaked at 90°. As discussed above, the lack of their detection could be the result of relatively low plasma densities and the warm background plasma. On balance, however, the evidence that a local current-driven instability is the source of the low-frequency plasma wave feature from $\sim$ 1446 to $\sim$ 1449 UT shown in Figure 5 is not very strong.

The second source of free energy that could generate the low-frequency plasma waves we are discussing is related to the specific shape of the downflowing ion distribution. We will demonstrate that a region of detectable downward flowing ions is observed to begin and end in close association with the observed banded ion feature seen from 1446 to 1449 UT. Figure 11 presents the EICS data for the interval from 1443 to 1450 UT in the form of an energy-time spectrogram. The data in Figure 11 are not presented in strict time order sequence; rather all of the energy-angle samples for each 24-s (i.e., 4 spin periods) instrumental cycle are plotted as a function of the pitch angle indicated in the bottom panel. In this format the EICS counting rates for hydrogen (top panel), oxygen (second panel), and from a detector sensitive to all ions (third panel) are encoded using the gray bar on the right. The EICS counting rates are approximately proportional to number flux. The most intense fluxes seen in Figure 11 are low-energy (i.e., less than 125 eV) upflowing ions seen at 180° pitch angle in all three panels. The downflowing ion event is seen in the top (hydrogen) and third (all ion) panels as an extended (in energy and pitch angle) intensification of the flux centered on zero degrees pitch angle and $\sim$ 1 keV at 1446 UT. During the event the center energy of the downflowing ion distributions falls to several hundred electron volts ending near 1450 UT. A second, less intense, energy-latitude dispersion of downflowing hydrogen ions is seen starting near 1448 UT at $\sim$ 1 keV.

Figure 12 displays the measured energetic hydrogen ion velocity distribution for eight equally spaced 6-s measurement periods from 1445:15 to 1450:51 UT in two different formats. The format of the contour plots in the top row was described in the discussion of Figure 7 above. (Note that the velocity range $\pm$ 1500 km/s includes hydrogen ions with energies less than $\sim$ 12 keV, and the 3-keV upper energy shown in the second format corresponds to a hydrogen velocity of $\sim$ 760 km/s) Two of the contour plots have been divided into eight sectors, and the sectors having the same pitch angle range have been labeled with pluses, asterisks, circles, and crosses. The average velocity space density for each of these four pitch angle ranges as a function of energy has been plotted below each contour in Figure 12 using the line code indicated at the bottom. The downward flowing hydrogen ion distribution appears as broad maxima in the energy spectra below 1 keV in the regularly spaced samples presented in Figure 12, between 1446:03 and 1450:03 UT. These broad maxima are found, in some cases, in the 90° to 135° pitch angle range, indicating that some of the observed downflowing ion distribution has been reflected by the converging magnetic field below the satellite. We note that a downward looking loss cone feature is present in the hydrogen velocity space distributions both before 1446 and after 1451 UT, and that "shell" shaped features, similar to those discussed by *Gorney* [1983], are detectable in some of the velocity space contour plots. We will discuss the implications of these observations below.

DISCUSSION

We have examined high-resolution ion mass spectrometer data and simultaneous low-frequency (less than 1000 Hz) plasma wave observations at mid-altitudes from the Dynamics Explorer 1 satellite. This examination was motivated by the desire to use the high-resolution, high-sensitivity data from the Dynamics Explorer 1 satellite to investigate the physical processes that impart energy to ionospheric ions transverse to magnetic field lines at high altitudes in the Earth's auroral zone.

One of the fundamental experimental problems in studying the transfer of energy from waves to particles is the difficulty in identifying regions where the transfer is occurring. In the mid-altitude auroral region sampled by the Dynamics Explorer 1 satellite, intense local regions of transverse ion energization characterized by 90° ion conic distributions were rarely observed. In the data surveyed for this report none of these unambiguous particle signatures of intense, local transverse ion energization were found. We therefore used two independent criteria to search for possible regions where ions were acquiring energy transverse to the local magnetic field. Specifically we searched for intervals in the data where local enhancements in both the low-frequency (less than 1 kHz) plasma wave emissions and in the ion temperature or pressure transverse to the magnetic field were found simultaneously. Of course the simultaneous occurrence of local maxima in

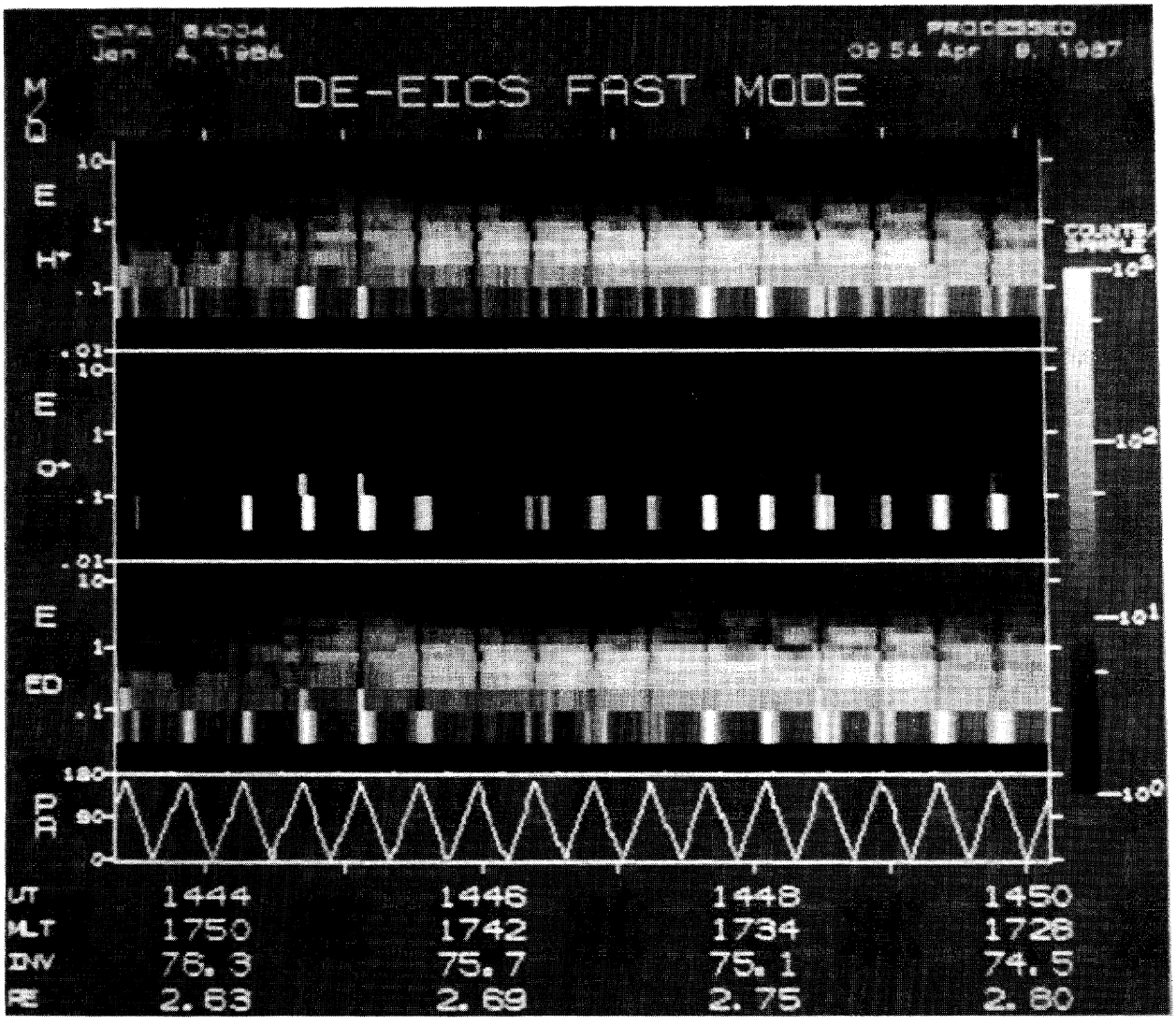

Fig. 11. EICS data for the interval from the indicated interval in the form of an energy-time spectrogram. The observed counting rates for hydrogen (top panel), oxygen (second panel), and from a detector sensitive to all ions (third panel) are encoded using the gray bar on the right. See text.

low-frequency wave and transverse ion energy does not uniquely identify regions where ions are acquiring transverse energy from plasma waves. It is reasonable, however, to use these two criteria to select intervals for more detailed study.

Intervals with near-simultaneous local maxima in low-frequency plasma wave emissions and partial perpendicular ion pressure were identified in a number of mid-altitude auroral zone crossings. Frequently the observations were consistent with the local transfer of transverse energy to ions. However, our search did not reveal a single event where we were able to show unambiguously that there was a significantly enhanced transfer of energy from plasma waves to ions. Because we do not yet know how to simply and compactly summarize the large volume of high-resolution data necessary to determine the plasma wave emission mode or shape of the ion velocity space distribution with the required temporal resolution, we elected to present high-resolution plasma measurements for only one crossing of the mid-altitude auroral zone.

We presented above a complete set of available high time resolution plasma measurements obtained from a high-altitude ($r/R_E \sim 3$) evening auroral zone pass and focused our attention on low-frequency (i.e., below $\sim$ 1000 Hz) plasma waves and ions with enhanced energies transverse to the local magnetic field. The low time resolution particle and wave data (Plate 1 and Figure 1) for the selected interval were shown to be typical of those seen on mid-altitude evening auroral zone crossings. The energy of upflowing energetic ions encountered was low ($\sim$ 100 eV), but this is consistent with the statistical studies of *Ghielmetti et al.* [1978], *Gorney et al.* [1981], and *Yau et al.* [1984] who reported less than 50% occurrence frequencies of upflowing energetic ions in the local time sector of the observations presented here. In the plasma wave data presented there were several intervals of emissions at or near multiples of the local hydrogen gyrofrequency. There were no detectable plasma wave emissions at or spaced at the oxygen ion gyrofrequency. Broadening effects introduced because of spacecraft velocity probably preclude the detection of plasma waves at the oxygen gyrofrequency at mid-auroral altitudes.

Low-frequency (less than 1 kHz) plasma waves were observed throughout the selected auroral zone crossing period. There were several short bursts of wave emission lasting on the order of one

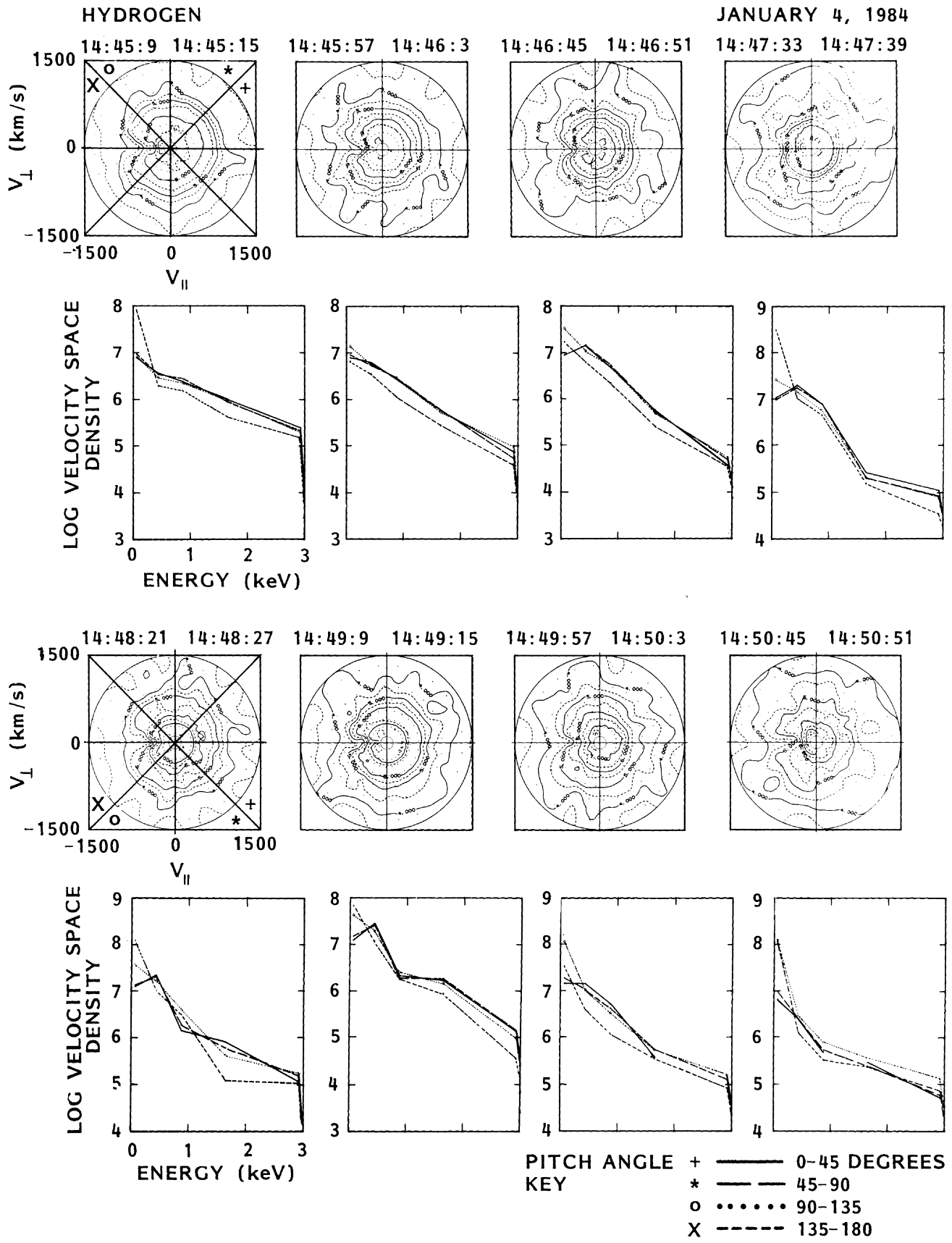

Fig. 12. Hydrogen ion velocity distribution for eight equally spaced 6-s measurement periods from 1445:15 to 1450:51 UT in two different formats. The contour plots in the top row have been described in Figure 7. Two of the contour plots have been divided into eight pitch angle sectors, and the sectors having the same pitch angle range have been labeled with pluses, asterisks, circles, and crosses. The average velocity space density for each of these four pitch angle ranges as a function of energy has been plotted below each contour using the line code indicated at the bottom. Note that hydrogen velocities of 760 and 1500 km/s correspond to energies of 3 and 12 keV respectively.

satellite spin period (6-s) or less. Because the cycle time of the particle instruments was longer than most of the low-frequency plasma wave emission features, and because of gradients in the ion density, only two regions were selected for detailed study. A third interval was chosen for detailed presentation because of a remarkably close association of an extended period of low-frequency emissions and downward flowing distributions of ions, an effect which has to date only been reported in the magnetospheric cusp region.

The rest of this discussion is organized as follows. We first summarize our unsuccessful attempts to unambiguously identify regions of transverse ion energization (i.e., heating or acceleration), followed by a discussion of other particle and wave features observed and not observed in the auroral zone crossing presented above.

Particle and Wave Signatures of Transverse Ion Heating or Acceleration

Given our present understanding of the interactions of ions with plasma waves, the only unambiguous particle signatures of local transverse ion energization are the so-called 90° ion conic distributions. Very few 90° conic ion distributions have been found in the EICS data to date; none have been found in the subset of the data for which wideband plasma wave observations are available. The infrequent observation of 90° conic ion distributions in the EICS data is consistent with earlier reports. Statistical studies of ion conics, not restricted to 90°, by *Gorney et al.* [1981] below 8000 km and *Yau et al.* [1984] from 8000 to 24,000 km, show a relatively constant frequency of occurrence from 2000 km to about 15,000 km. Below ~ 2000 and above ~ 15,000 km the occurrence frequency of conics falls off. There are no published reports of the mid- and high-altitude distribution of 90° conic events, which are sometimes referred to as transversely accelerated ions (TAI's). TAI's are a common feature on auroral field lines at altitudes below 3000 km (see, for example, *Klumpar* [1979], and *Yau et al.* [1983]). At S3-3 altitudes (i.e., below 8000 km), several hundred 90° conic events were observed (D. J. Gorney, private communication, 1987). Infrequent observations of 90° conics have also been made at altitudes of 2.5 to 6.5 Earth radii in the auroral zone from ISEE 1 (C. Cattell and W. Lennartsson, private communication, 1987).

The infrequent observation of 90° ion conic distributions at the altitudes sampled by DE 1 is consistent with at least three interpretations: (1) regions of transverse energization frequently result in 90° ion conics, but the physical extent of transverse energization regions is small and therefore infrequently sampled by satellites at these altitudes; (2) transverse ion energization rarely occurs in the absence of other processes or over restricted altitude ranges at these altitudes; or (3) transverse ion energization occurs, but the energies and intensities of the heated ions are below the threshold of detection of existing instrumentation. Based on our present knowledge it is difficult to dismiss any of these interpretations.

Recently the observations of *Klumpar et al.* [1984] have pointed out that not all transverse ion acceleration events result in particle distributions that peak in a direction perpendicular to the local magnetic field. *Klumpar et al.* [1984] interpreted their results in terms of a bimodal acceleration, i.e., both transverse and parallel acceleration occurring on the same field line and near the same altitude. Observations of *Chang et al.* [1986] of ion distributions similar to those reported by Klumpar et al. have been interpreted in terms of an entirely new type of transverse ion energization mechanism, one that operates over an extended altitude region and is driven by the intense, broadband background of low-frequency plasma waves encountered on auroral field lines.

In the absence of the identification of intervals where the plasma data unambiguously show that energy is being locally transferred from the waves to the particles, we have searched the data and found several regions where the data are consistent with such transfer. Two of those intervals were in the mid-altitude auroral zone crossing selected for detailed presentation in this report: specifically the intervals on January 4, 1984, near 1439 and 1442:30 UT.

The evidence for local heating of the ions near 1439 and 1442:30 UT by ion cyclotron waves arising from a local current-driven instability presented above is incomplete. The lack of observational constraints on the thermal electron distribution from instrumentation on the DE 1 satellite or from the very few spacecraft that have sampled auroral zone plasmas in the 2 to 4 r/R_E region and the lack of an unambiguous identification of the plasma emission mode limit the conclusions that can be drawn from the assembled data. We did not find a well-defined ion distribution peaking perpendicular to the magnetic field at these times. This so-called 90° conic signature is expected at the location of a current-driven plasma instability (see, for example, *Kintner and Gorney* [1984]). We pointed out that a small component of locally produced ions at 90° pitch angle could have been present but masked by a larger population of ions heated or energized perpendicular to the magnetic field up to 1000 km below the satellite, and that these ions could be driving the low-frequency plasma waves observed at the time (see, for example, *Andre et al.* [1986]).

Finally, we point out that the one-dimensional hydrogen velocity space distributions presented in Figure 8 by themselves suggest local perpendicular energization of the hydrogen near 1439 UT. Detailed examination of the two-dimensional velocity space distributions in Figure 7 leads to the much weaker conclusion presented above.

Other Particle and Wave Features in the Data from January 4, 1984

In addition to the two intervals near 1439 and 1442:30 UT that satisfied the joint wave and particle criteria, there are at least three other intervals in the data presented above that have extended periods of intense low-frequency wave emissions, 1440 to 1441, near 1445, and from ~ 1446 to 1449 UT (Figure 5). Complete high resolution plasma data have been presented above only for the last interval.

The first two intervals (1440 to 1441 and near 1445 UT) are characterized by gradients in the hydrogen ion plasma. The plasma waves observed from 1440 to 1441 UT are at or below the lower hybrid resonance frequency but well above the local hydrogen gyrofrequency. There is a sharp gradient in the thermal (less than 10 eV) ion density (Figure 3) between 1440 and 1441 UT. The low-frequency plasma waves observed near 1445 are distinctly different from those observed from 1440 to 1441 UT. The density gradient observed near 1445 UT is in the energetic (greater than 150 eV) ion plasma. The energetic ion density gradient can be seen both in Figure 3, and in Figure 2 where the partial hydrogen perpendicular temperature is approximately constant, but the partial hydrogen perpendicular pressure (which is proportional to the density times the temperature) has a sharp gradient. Transverse ion energization is undoubtedly occurring during

both density gradient intervals. It is, however, nearly impossible to identify the contribution of transverse ion energization to the measured ion velocity space distributions from ion heating in the presence of these density gradients. The plasma waves associated with these density gradients are worthy of further investigation, but such a study is beyond the scope of this paper.

We have presented above complete high-resolution ion plasma data for the interval 1446 to 1449 UT. These data demonstrate that the distinctive banded plasma wave emission feature (Figure 5) is closely associated with a downward flowing hydrogen ion distribution (Figures 11 and 12). This observation is remarkable for two reasons. First, there have been relatively few reports of downward flowing ion distributions outside the cusp region. Second, it is unusual to obtain such a close association of simultaneous features in both plasma wave emissions and ion velocity space distributions on mid-altitude auroral field lines.

Downward flowing ion distributions have been infrequently reported outside the cusp region because of the difficulty in identifying them in the presence of the hot background plasma distribution typically found on auroral field lines (see, for example, *Ghielmetti et al.* [1979]). Two source regions for downward flowing ion distributions such as those shown in Figures 11 and 12 have been identified by *Quinn and McIlwain* [1979], near the equator and in the magnetically conjugate ionosphere. *Winningham et al.* [1984], *Bosqued et al.* [1986], and *Frahm et al.* [1986] have shown that upflowing ion beams from the magnetically conjugate hemisphere can, under the proper conditions, be detected from a satellite just above the ionosphere. All of these workers report an energy-latitude dispersion in the energy of the peak flux similar to those shown in Figure 11. *Quinn and McIlwain* [1979] and *Klumpar et al.* [1983] have presented downflowing ion distributions similar to those shown in Figures 11 and 12 and demonstrated that they originated from an impulsive event (i.e., a time scale short compared to the ion bounce period) located near the magnetic equator. We have not determined the origin of the downflowing ion distribution reported here.

Banded emissions of low-frequency plasma waves at and below the lower hybrid resonance frequency spaced at the hydrogen gyrofrequency have been reported in the dayside cusp and auroral regions from the S3-3, Dynamics Explorer and Viking satellites [*Gorney*, 1983; *Cattell and Hudson*, 1982; *Andre et al.* 1986; *Peterson et al.*, 1986; *Koskinen et al.*, 1987]. Several free energy sources for these plasma wave emissions have been suggested. These include the ion loss cone and, magnetic focusing of ion conic distributions, as well as ion velocity distributions associated with beams of ions flowing down converging magnetic field lines. *Gorney* [1983] pointed out that downflowing ion distributions similar to those shown in Figures 11 and 12, which occur regularly in the dayside cusp region of the magnetosphere, can lead to the generation of low-frequency plasma waves which in turn can transversely accelerate or heat a local low-energy plasma population. *Roth and Hudson* [1985] quantitatively considered transverse ion energization driven by downflowing ring or shell distributions of solar wind hydrogen and doubly charged helium ions in the dayside cusp region. Roth and Hudson were able to reproduce most of the observed characteristics of the plasma waves and of ion heating in the dayside cusp region in their simulation model. *Andre* [1986] argued that waves such as those seen from 1446 to 1449 UT could be driven by an ion loss cone velocity distribution. *Andre et al.* [1986] were able to reproduce most of the wave emission features of an event similar to the one presented here using an ion distribution with both loss cones and a magnetically folded upflowing ion conic distribution.

Since it is experimentally difficult to detect downward flowing ion distributions outside the cusp region and the direct relationship between plasma wave emissions and downflowing ion distributions has not been established outside the cusp region, we have investigated the uniqueness of the close association between the wave and particle features found between 1446 and 1450 UT discussed here. We first selected several intervals from other auroral zone crossings outside the cusp region where extended plasma wave features such as those seen between 1446 and 1449 UT in Figure 5 were observed. The ion distributions found in these intervals were diverse. We detected intervals of downward flowing ions in some, but not all, periods. Some, but not all, of the intervals of downflowing ions corresponded closely to the selected region of plasma wave emissions. Because downward flowing ion distributions are difficult to find outside the cusp region, we have not done the control experiment; i.e., first identify a downward flowing ion distribution and then look at the plasma wave emission spectra. In any case the above observations demonstrate that downward flowing ion distributions are neither a necessary nor a sufficient condition for the generation of the observed banded wave spectra.

In the data for January 4, 1984, presented above we found no evidence for lower hybrid mode ion heating. *Chang and Coppi* [1981] have argued that transfer of energy from electrons to ions is very efficient through plasma wave modes in the frequency range of the ion plasma frequency. *Kintner and Gorney* [1984] found that lower hybrid waves were probably the cause of local ion heating (identified by the presence of a 90° ion conic) at 2400 km in the one case with simultaneous wideband plasma wave data they were able to find in the S3-3 data set. The expected wave signature of a source of lower hybrid plasma wave emissions is a region with intense emissions above the lower hybrid resonance frequency whose lower-frequency cutoff increases with distance away from the source. Plasma wave emissions observed above the lower hybrid resonance frequency were weak and sporadic compared to the emissions below the lower hybrid resonance frequency. The observations presented here do not rule out the possibility of transverse energization driven by plasma waves above the lower hybrid resonance frequency at lower altitudes, and transport of the ions to higher altitudes under the influence of the magnetic mirror force, as pointed out by *Chang and Coppi* [1981].

We did not address the possibility of ion acceleration resulting from the drift of ions across oblique double layers as discussed by *Borovsky* [1984] because the dc electric field measurements are not fully three dimensional and the predominant direction of ion drift in our case is parallel to, not across, the auroral oval. Finally, we must note that the DE 1 orbit is not the only one from which to study transverse ion acceleration and energization at mid- auroral altitudes. The ~ 24,000-km apogee and 90° inclination of the DE 1 orbit result in crossings of the auroral zone that are quite rapid compared to instrumental cycle times at low (i.e., below ~ 8000 km) altitudes. Above 8000 km, the satellite crosses the auroral zone in a period of minutes. The ISEE 1 spacecraft, with an apogee of over 20 Earth radii and an orbit plane inclined to the ecliptic, traversed auroral field lines more slowly. *Ungstrup et al.* [1984] have in fact documented the time evolution of an ion conic distribution produced at ionospheric altitudes as it flows past the ISEE 1 spacecraft at an altitude of 10,300 km. The DE 1 orbit does result in extended periods when the satellite remains on the same field line, but because of the relatively low apogee, the magnetic field line is on an "L" shell near 4 (invariant latitude near 60°) which is equatorward of magnetic field lines where most of the transverse ion energization and acceleration occur.

CONCLUSIONS

Transverse ion acceleration and/or energization on auroral field lines is a fundamental process that provides energy to ionospheric ions and allows them to populate all regions of the magnetosphere. The high- sensitivity and high resolution data obtained by the Dynamics Explorer 1 satellite presented in this report illustrate the variety of plasma wave emission features and the short temporal and/or spatial scales of the particle environment encountered at mid-altitudes in the auroral zone. We were unable to unambiguously identify in these data a region where energy was locally transferred to ions from the plasma waves, which illustrates the complexities of understanding the transfer of energy between plasma waves and ions in the auroral environment.

Acknowledgments. We want to thank Ann Persoon for providing some of the density data presented in Figure 3, and C. R. Chappell for permission to use the RIMS data. This research was supported by the NASA under contract NAS5-28710 at Lockheed and grants NAG5-310, and NGL 16-001-043 at the University of Iowa.

The Editor thanks J. F. Fennell and E. Ungstrup for their assistance in evaluating this paper.

REFERENCES

Andre, M., Electrostatic ion waves generated by ion loss-cone distributions in the magnetosphere, *Ann. Geophys., 4*, 241, 1986.

Andre, M., M. Temerin, and D. Gorney, Resonant generation of ion waves on auroral field lines by positive slopes in ion velocity space, *J. Geophys. Res., 91*, 3145, 1986.

Ashour-Abdalla, M., D. Schriver, and H. Okuda, Transverse ion heating in multicomponent plasmas along auroral zone field lines, *J. Geophys. Res.*, in press, 1988.

Bergmann, R., Electrostatic ion (hydrogen) cyclotron and ion acoustic wave instabilities in regions of upward field-aligned current and upward ion beams, *J. Geophys. Res., 89*, 953, 1984.

Borovsky, J. E., The production of ion conics by oblique double layers, *J. Geophys. Res., 89*, 2251, 1984.

Bosqued, J. M., J. A. Sauvaud, K. Delcourt, and R. A. Kovrazhkin, Precipitation of suprathermal ionospheric ions accelerated in the conjugate hemisphere, *J. Geophys. Res., 91*, 7006, 1986.

Cattell, C., The relationship of field-aligned currents to electrostatic ion cyclotron waves, *J. Geophys. Res., 86*, 3641, 1981.

Cattell, C., and M. Hudson, Flute mode waves near ω_{LH} excited by ion rings in velocity space, *Geophys. Res. Lett., 9*, 1167, 1982.

Chang, T., and B. Coppi, Lower hybrid acceleration and ion evolution in the suprauroral region, *Geophys. Res. Lett., 8*, 1253, 1981.

Chang, T., G. B. Crew, N. Hershkowitz, J. R. Jasperse, J. M. Retterer, and J. D. Winningham, Transverse acceleration of oxygen ions by electromagnetic ion cyclotron resonance with broad band left-hand polarized waves, *Geophys. Res. Lett., 13*, 636, 1986.

Chappell, C. R., S. A. Fields, C. R. Baugher, J. H. Hoffman, W. B. Hanson, W. W. Wright, H. D. Hammack, G. R. Carignan, and A. F. Nagy, The retarding ion mass spectrometer on Dynamics Explorer -A, *Space Sci. Instrum., 5*, 477, 1981.

Collin, H. L., and R. G. Johnson, Some mass dependent features of energetic ion conics over the auroral regions, *J. Geophys. Res., 90*, 9911, 1985.

Farthing, W. H., M. Sugiura, B. G. Ledley, and L. J. Cahill, Jr., Magnetic field observations on DE-A and -B, *Space Sci. Instrum., 5*, 551, 1981.

Frahm, R. A., P. H. Reiff, J. D. Winningham, and J. L. Burch, Banded ion morphology: Main and recovery storm phases, in *Ion Acceleration in the Magnetosphere and Ionosphere, Geophys. Monogr. Ser.*, vol. 38, edited by T. Chang, p. 98, AGU, Washington, D. C., 1986.

Gallagher, D. L., J. D. Menietti, J. L. Burch, A. M. Persoon, J. H. Waite, Jr., and C. R. Chappell, Evidence of high densities and ion outflows in the polar cap during the recovery phase, *J. Geophys. Res., 91*, 3321, 1986.

Ghielmetti, A. G., R. G. Johnson, R. D. Sharp, and E. G. Shelley, The latitudinal, diurnal and altitudinal distributions of upward flowing energetic ions of ionospheric origin, *Geophys. Res. Lett., 5*, 59, 1978.

Ghielmetti, A. G., R. D. Sharp, E. G. Shelley and R. G. Johnson, Downward flowing ions and evidence for injection of ionospheric ions into the plasma sheet, *J. Geophys. Res., 84*, 5781, 1979.

Gorney, D. J., An alternative interpretation of ion ring distributions observed by the S3-3 satellite, *Geophys. Res. Lett., 10*, 417, 1983.

Gorney, D. J., A. Clarke, D. Croley, J. Fennell, J. Luhmann, and P. Mizera, The distribution of ion beams and conics below 8000 km, *J. Geophys. Res., 86*, 83, 1981.

Gurnett, D. A., S. D. Shawhan, and R. R. Shaw, Auroral hiss, *Z* mode radiation, and auroral kilometric radiation in the polar magnetosphere: DE 1 observations, *J. Geophys. Res., 88*, 329, 1983.

Hoffman, R. A., G. D. Hogan, and R. C. Maehl, Dynamics Explorer spacecraft and ground operations systems, *Space Sci. Instrum., 5*, 349, 1981.

Iijima, T., and T. A. Potemra, Large-scale characteristics of field-aligned currents associated with substorms, *J. Geophys. Res., 83*, 599, 1978.

Kaufmann, R. L., and P. M. Kintner, Upgoing ion beams; 1, Microscopic analysis, *J. Geophys. Res., 87*, 10,487, 1982.

Kindel, J. M., and C. F. Kennel, Topside current instabilities, *J. Geophys. Res., 76*, 3055, 1971.

Kintner, P. M., On the distinction between electrostatic ion cyclotron waves and ion cyclotron harmonic waves, *Geophys. Res. Lett., 7*, 585, 1980.

Kintner, P. M., Experimental identification of electrostatic plasma waves within ion conic acceleration regions, in *Ion Acceleration in the Magnetosphere and Ionosphere, Geophys. Monogr. Ser.*, vol. 38, edited by T. Chang, p. 384, AGU, Washington, D. C., 1986.

Kintner, P. M., and D. G. Gorney, A search for the plasma processes associated with perpendicular ion heating, *J. Geophys. Res., 89*, 937, 1984.

Kintner, P. M., M. C. Kelley, and F. S. Mozer, Electrostatic hydrogen cyclotron waves near one Earth radius altitude in the polar magnetosphere, *Geophys. Res. Lett., 5*, 139, 1978.

Klumpar, D. M., Transversely accelerated ions: An ionospheric source of hot magnetospheric ions, *J. Geophys. Res, 84*, 4229, 1979.

Klumpar, D. M., A digest and comprehensive bibliography on transverse auroral ion acceleration, in *Ion Acceleration in the Magnetosphere and Ionosphere, Geophys. Monogr. Ser.*, vol. 38, edited by T. Chang, p. 389, AGU, Washington, D. C., 1986.

Klumpar, D. M., W. K. Peterson, E. G. Shelley, and J. M. Quinn, Localized magnetospheric ion injection outside the cusp, *Eos Trans. AGU, 64*, 297, 1983.

Klumpar, D. M., W. K. Peterson, and E. G. Shelley, Direct evidence for two-stage (bimodal) acceleration of ionospheric ions, *J. Geophys. Res., 89*, 10,779 1984.

Koskinen, H. E. J., P. M. Kintner, G. Holmgren, B. Holback, G. Gustafsson, M. Andre, and R. Lundin, Observations of ion cyclotron harmonic waves by the Viking satellite, *Geophys. Res. Lett., 14*, 459, 1987.

Lysak, R. L., Ion acceleration by wave-particle interaction, in *Ion Acceleration in the Magnetosphere and Ionosphere, Geophys. Monogr. Ser.*, vol. 38, edited by T. Chang, p. 261, AGU, Washington, D. C., 1986.

Lysak, R. L., M. K. Hudson, and M. Temerin, Ion heating by strong electrostatic ion cyclotron turbulence, *J. Geophys. Res., 85*, 678, 1980.

Mitchell, H. G., and P. J. Palmadesso, A dynamic model for the auroral field line plasma in the presence of field-aligned current, *J. Geophys. Res., 88*, 2131, 1983.

Nagai, T., J. H. Waite, Jr., J. L. Green, C. R. Chappell, R. C. Olsen, and R. H. Comfort, First measurements of the supersonic polar wind in the polar magnetosphere, *Geophys. Res. Lett., 11*, 669, 1984.

Olsen, R. C., C. R. Chappell, and J. L. Burch, Aperture plane potential control for thermal ion measurements, *J. Geophys. Res., 91*, 3117, 1986.

Persoon, A. M., D. A. Gurnett, and S. D. Shawhan, Polar cap electron densities from DE 1 plasma wave observations, *J. Geophys. Res., 88*, 10,123, 1983.

Persoon, A. M., D. A. Gurnett, W. K. Peterson, J. H. Waite, Jr., J. L. Burch, and J. L. Green, Electron density depletions in the nightside auroral zone, *J. Geophys. Res., 93*, 1871, 1988.

Peterson, W. K., E. G. Shelley, S. A. Boardsen, and D. A. Gurnett, Transverse auroral ion energization observed on DE 1 with simultaneous plasma wave and ion composition measurements, in *Ion Acceleration in the Magnetosphere and Ionosphere, Geophys. Monogr. Ser.*, vol. 38, edited by T. Chang, p. 43, AGU, Washington, D. C., 1986.

Quinn, J. M., and C. E. McIlwain, Bouncing ion clusters in the Earth's magnetosphere, *J. Geophys. Res., 84*, 7365, 1979.

Roth, I., and M. K. Hudson, Lower hybrid heating of ionospheric ions due to ion ring distributions in the cusp, *J. Geophys. Res., 90*, 4191, 1985.

Sharp, R. D., R. G. Johnson, and E.G. Shelley, Observation of an ionospheric acceleration mechanism producing energetic (keV) ions primarily normal to the geomagnetic field direction, *J. Geophys. Res., 82*, 3324, 1977.

Sharp, R. D., D. L. Carr, W. K. Peterson, and E. G. Shelley, Ion streams in the magnetotail, *J. Geophys. Res., 86*, 4639, 1981.

Shawhan, S. D., D. A. Gurnett, D. L. Odem, R. A. Helliwell, and C. G. Park, The plasma wave and quasi-static electric field instrument (PWI) for Dynamics Explorer-A, *Space Sci. Instrum., 5*, 535, 1981.

Shelley, E. G., Magnetospheric energetic ions from the Earth's ionosphere, *Adv. Space Res., 6*, 121, 1986.

Shelley, E. G., D. A. Simpson, T. C. Sanders, E. Hertzberg, H. Balsiger, and A. Ghielmetti, The energetic ion composition spectrometer (EICS) for the Dynamics Explorer-A, *Space Sci. Instrum., 5*, 443, 1981.

Temerin, M., Evidence for a large bulk ion conic heating region, *Geophys. Res. Lett., 13*, 1059, 1986.

Ungstrup, E., D. M. Klumpar, and W. J. Heikkila, Heating of ions to superthermal energies in the topside ionosphere by electrostatic cyclotron harmonic waves, *J. Geophys. Res., 84*, 4289, 1979.

Ungstrup, E., R. D. Sharp, C. A. Cattell, R. R. Anderson, R. J. Fitzenreiter, D. S. Evans, and D. N. Baker, Observation of a westward traveling surge from satellites at low, medium and high altitudes, *Rep. 2-84*, Danish Space Res. Inst., Lyngby, 1984.

Yau, A. W., B. A. Whalen, A. G. McNamara, P. J. Kellog, and W. Bernstein, Particle and wave observations of low-altitude ionospheric ion acceleration events, *J. Geophys. Res., 88*, 341, 1983.

Yau, A. W., B. A. Whalen, W. K. Peterson, and E. G. Shelley, Distribution of upflowing ionospheric ions in the high-altitude polar cap and auroral ionosphere, *J. Geophys. Res., 89*, 5507, 1984.

Yau, A. W., P. H. Beckwith, W. K. Peterson, and E. G. Shelley, Long-term (solar cycle) and seasonal variations of upflowing ionospheric ion events at DE 1 altitudes, *J. Geophys. Res., 90*, 6395, 1985*a*.

Yau, A. W., E. G. Shelley, W. K. Peterson, and L. Lenchyshyn, Energetic auroral and polar ion outflow at DE 1 altitudes: Magnitude, composition, magnetic activity dependence, and long-term variations, *J. Geophys. Res., 90*, 8417, 1985*b*.

Winningham, J. D., J. L. Burch, and R. A. Frahm, Bands of ions and angular V's: A conjugate manifestation of ionospheric ion acceleration, *J. Geophys. Res., 89*, 1749, 1984.

S. A. Boardsen and D. A. Gurnett, University of Iowa, Iowa City, IA 52242.

B. G. Ledley, NASA Goddard Space Flight Center, Greenbelt, MD 20771.

T. E. Moore, NASA Marshall Space Flight Center, Huntsville, AL 35812.

W. K. Peterson and E. G. Shelley, Lockheed Research and Development, 91-20, Building 255, 3251 Hanover Street, Palo Alto, CA 94304.

M. Sugiura, Geophysical Institute, Kyoto University, Kyoto 606, Japan.

J. H. Waite, Jr., Department of Space Sciences, Southwest Research Institute, 6220 Culebra Road, P. O. Drawer 28510, San Antonio, TX 78284.

(Received January 15, 1988;
revised May 5, 1988;
accepted May 9, 1988.)